High Fidelity VSF Measurements and Inversion for RaDyO (Hi Fi RaDyO)

Michael Twardowski
Department of Research
WET Labs, Inc.
70 Dean Knauss Dr
Narragansett, RI 02882
phone: (401)783-1787 fax: (401)783-0309 email: mtwardo@wetlabs2.com

Ron Zaneveld
Department of Research
WET Labs, Inc.
620 Applegate St
Philomath, OR 97370
phone: (541)929-5650 fax: (541)929-5277 email: ron@wetlabs.com

Contract Number: N0001406C0027
http://www.wetlabs.com

LONG TERM GOALS

Time and space dependent radiance distributions at the sea surface are a function of the shape of the incident distribution on the surface, modification by the sea surface itself from topography and transmission characteristics, and alteration by the Inherent Optical Properties (IOPs) of the surface ocean. Our long term goal is understanding this last controlling factor. With a knowledge of the IOPs, radiance fields can be directly computed from the incident field using the equation of radiative transfer, now embedded in commercially available code (e.g., Hydrolight).

With the state of current technology and methodologies, the primary obstacles in understanding subsurface IOPs and their high-frequency dynamics are a lack of 1) volume scattering instrumentation, 2) comprehensive inversion models linking the IOPs with the ambient particle fields including bubbles (models which in many cases will require input dependent on 1), and 3) suitably stable, non-intrusive platforms to sample the subsurface ocean. The first two challenges are addressed in this project.

OBJECTIVES

There are two broad objectives for this project:

1) To develop an in-situ volume scattering function device measuring volume scattering from 10° to 170° at 10° intervals and sampling rates of 1 s^{-1} or better to sample the VSF in near-surface waters; and

2) To develop and refine IOP inversion models to resolve particle field characteristics on small spatial (cm's) and temporal (<1 s) scales in near-surface waters.

Report Documentation Page

Form Approved
OMB No. 0704-0188

1. REPORT DATE	2. REPORT TYPE	3. DATES COVERED
2009		**00-00-2009 to 00-00-2009**

4. TITLE AND SUBTITLE	5a. CONTRACT NUMBER
High Fidelity VSF Measurements and Inversion for RaDyO (Hi Fi RaDyO)	5b. GRANT NUMBER
	5c. PROGRAM ELEMENT NUMBER
6. AUTHOR(S)	5d. PROJECT NUMBER
	5e. TASK NUMBER
	5f. WORK UNIT NUMBER
7. PERFORMING ORGANIZATION NAME(S) AND ADDRESS(ES) **WET Labs, Inc,Department of Research,70 Dean Knauss Dr,Narragansett,RI,02882**	8. PERFORMING ORGANIZATION REPORT NUMBER
9. SPONSORING/MONITORING AGENCY NAME(S) AND ADDRESS(ES)	10. SPONSOR/MONITOR'S ACRONYM(S)
	11. SPONSOR/MONITOR'S REPORT NUMBER(S)

12. DISTRIBUTION/AVAILABILITY STATEMENT
Approved for public release; distribution unlimited

13. SUPPLEMENTARY NOTES

14. ABSTRACT

15. SUBJECT TERMS

16. SECURITY CLASSIFICATION OF:			17. LIMITATION OF ABSTRACT	18. NUMBER OF PAGES	19a. NAME OF RESPONSIBLE PERSON
a. REPORT **unclassified**	b. ABSTRACT **unclassified**	c. THIS PAGE **unclassified**	**Same as Report (SAR)**	**38**	

APPROACH

Our design for the VSF device is illustrated in **Figure 1**. The device is called MASCOT (Multi-Angle SCattering Optical Tool). The source beam is a 30 mW 658 nm laser diode expanded with a Gallilean 2X beam expander to an approximately 3 mm X 8 mm elliptical shape. A wedge depolarizer is used to provide the unpolarized light needed for VSF determinations. Seventeen independent silicon diode detectors spaced in a semicircle 10 cm around the sample volume measure volume scattering from 10° to 170° at 10° intervals. The total pathlength for all scattering measurements is 20 cm. Independent detectors allow resolution of the VSF without any moving parts and time-consuming scanning. Additionally, each detector can be optimized for its specific dynamic range. Detector field-of-views (FOVs) range from 0.8° to 5° for the different detectors, with the narrowest FOVs associated with the detectors measuring scattering in the forward direction. Using proprietary electronics, a 20 Hz sampling rate for all channels has been achieved while maintaining a worst case signal:noise of 300:1. Relatively fast sampling rates are important in resolving VSFs in the highly dynamic ocean subsurface.

Polarized VSFs have now been successfully collected with the addition of filter mount placed in front of the source beam. A linear polarizer is used to obtain scattering from a vertically and horizontally polarized source (in terms of the Mueller scattering matrix elements, (S11+S12)/2 and (S11-S12)/2 are measured, so that S11 and S12 may be derived). Adding polarized scattering increases the amount of information on particle characteristics we are collecting, and is expected to improve our ability to discriminate different particle types (both the number of subpopulations and the accuracy of individual determinations). The degree of linear polarization (S12/S11) is most dependent on the degree of sphericity, particle size, and refractive index composition.

For VSF inversion modeling, we are extending the capabilities of existing models (Twardowski et al. 2001; Twardowski and Zaneveld, 2004; Zhang et al. 2005) by incorporating input from new VSF measurements and by adding bubble particle populations (clean and coated) in the models. Candidate phase functions for particle subpopulations are fit to measured VSFs using a least-squares minimization procedure. These phase functions can be obtained theoretically using Mie theory, DDA, or FDTD techniques, or experimentally in controlled laboratory conditions.

The MASCOT has now been extensively deployed concurrently with the commercially available near-forward VSF device LISST (Sequoia Inc.) in order to capture the VSF with good resolution from ~0.1 degrees to 170 degrees. Our deployment package also contains CTD, AC9 (or ACS), and various ECO scattering sensors, all integrated in a real-time vertical profiling system (**Fig. 2)**.

Deployments for RaDyO have taken place in collaboration with other RaDyO investigators off Scripps Pier in January 2008, in Santa Barbara Channel in September 2008, and are ongoing off Hawaii at this time. For these RaDyO deployments, we have also intermittently integrated two additional sensors: 1) a high sampling rate fish-eye lens radiometer currently being developed by Marlon Lewis and Scott McLean of Satlantic, and 2) a bubble acoustic resonator developed by Svein Vagle, David Farmer, and Helen Czerski. For the Scripps Pier experiment, a mobile deployment platform was configured so that measurements could be made along the length of the pier, with the expectation that higher concentrations of bubbles would be observed nearing the surfzone. For subsequent field work in SBC and Hawaii, we are deploying our sensor package off the R/V Kilo Moana.

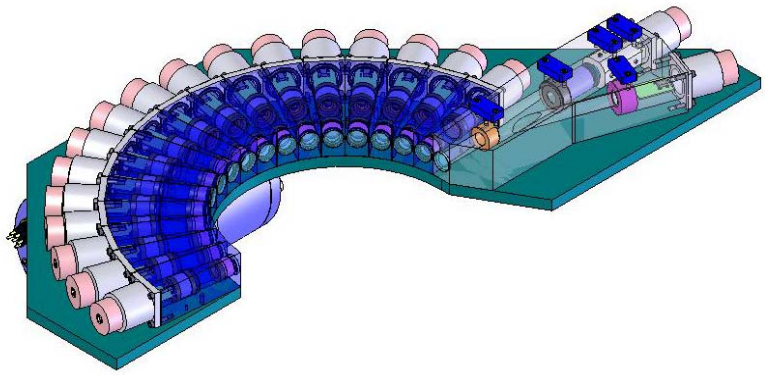

Figure 1. Oblique view illustration of the MASCOT. The VSF is resolved from 10 to 170 degrees in 10 degree intervals. Detectors are wedge shaped and arranged in a semi-circle on an aluminum frame to minimize reflections and perturbation of the water sample in the remote volume (center of semi-circle). The source assembly includes a 30 mW 658 nm laser diode, reference detector, beam expander, and wedge depolarizer. Wiring from all the detector modules and the source module feeds to a data handling unit.

WORK COMPLETED

- An IOP package including the MASCOT and LISST was deployed off Scripps Pier, in the Santa Barbara Channel, and off Hawaii during collaborative RADYO exercises.
- The MASCOT was adapted to additionally measure linear polarized scattering elements to derive degree of linear polarization (DOLP) as a function of angle.
- An acoustic bubble resonator (Vagle and Farmer) and a fish-eye lens camera (Lewis) were successfully integrated on the MASCOT IOP package and deployed periodically for all exercises.
- The MASCOT IOP package was also tested off the New York bight in May and July in association with other funded work.
- A revised calibration protocol was developed and implemented, using clean techniques and accurately accounting for pure water absorption along the optical path.
- A revised calibration and correction protocol was developed for the LISST to account for ambient light contamination, turbulent scattering, and vignetting
- A second MASCOT prototype with a larger dynamic range suitable for high turbidity environments (such as the surf zone) was tested in the lab and deployed in the NY bight.
- Inversion of MASCOT VSFs collected off Scripps Pier and the SBC into component VSFs associated with subpopulations of the bulk particle field including bubbles has been refined using a least-squares minimization model based on Mie theory, including derivation of particle concentration and size distribution for each subpopulation. We are currently adapting this model to also invert for nonspherical asymmetric polyhedron particles more analogous to natural suspended mineral populations.
- 3 papers are in prep and 1 was just accepted that are based on our results from this project.

RESULTS

Fig. 2 shows the MASCOT device in a custom cage with additional optical sensors ready for deployment. Orientation in the horizontal plane minimizes any shear perturbation of the sampled water parcel during upcasts.

Scripps Pier. **Fig. 3** shows scattering results from our deployment of the MASCOT off Scripps Pier in January. Typically, waves breaking shoreward of the sensor package's location produced suspended sediment and bubble plumes that became entrained in a seaward rip current running along the south side of the pier where the sensor package was suspended. Bubble plumes had a visible reflectance expression for several seconds, while discrete suspended sediment plumes were clearly observed lasting for up to minutes. At high tide (the condition at the beginning of the **Fig. 3** time series), with the surf zone far shoreward of our position (>100 m), plumes with injected air bubbles typically did not persist long enough to reach our sensors, although episodic local breaking with localized bubble injection did occasionally occur. In these conditions, periodic plumes of suspended sediment entrained in the seaward rip current were clearly visible as turbidity maxima with a distinct VSF character (greater relative backscattering than the background). As the tide ebbed, the surf zone passed directly through our sampling region so that plumes of both bubbles and sediments were sampled. Plumes dominated with bubble particles exhibited a well-known enhancement in scattering at mid-angles, from 60 to 90 degrees (e.g., Zhang et al. 2004). This is the first time this mid-angle enhancement in scattering due bubbles has been observed in-situ. The 20 Hz sampling rate for all VSF channels allows sufficient resolution of the bubble plumes as they rapidly evolve in time and space. A very low background scattering condition (particle attenuation less than 0.3 m^{-1} at 532 nm) enhanced our dynamic range in resolving intense scattering associated with episodic bubble and sediment plume generation.

A library of VSFs generated from a coated Mie theory model representing 180 initial particle subpopulations were fitted to measured VSFs using a least-squares minimization technique (see **Fig. 4** for details). This work has been carried out in collaboration with Xiaodong Zhang at the U. of N. Dakota. **Fig. 5** shows inversion results for combined bubble subpopulations and combined mineral populations. Results are encouraging and are consistent with anecdotal evidence (what we saw) with respect to patches of sediment and/or bubbles. **Fig. 6** shows the inversion results for the 2 primary bubble subpopulations, and **Fig. 7** shows results for the primary mineral subpopulations. **Fig. 8** shows acoustics data collected with the Svein/Farmer bubble resonator concurrently with the MASCOT VSF data for the last 40 minutes of the **Fig. 3** time series. Good agreement between patterns in optical scattering from bubbles (positive displacements of the $\beta(60)/\beta(120)$ relationship relative to the background) and acoustic attenuation at multiple frequencies was observed, but the agreement was even better when comparing with the large bubble subpopulation from the inversion results. **Fig. 9** shows the size distributions from the inversion results, with an aggregate distribution consistent with the familiar Junge-type distribution in the optically relevant size range (~0.1 to ~40 μm). Stable model solutions (only possible to assess with a very large number of VSFs) consistent with anecdotal observations of particle composition, coupled with validation based on acoustic measurements of bubble distributions and fractional and aggregate size distributions agreeing with theory and observations, provides strong evidence that our inversion results are environmentally meaningful.

Santa Barbara Channel. During the recent Santa Barbara Channel experiment, over 150 casts or time series were collected, including, for the first time, polarized scattering elements with quasi-concurrent

measurements of dark offsets to ensure the greatest accuracy possible. Plots of attenuation, chlorophyll, backscattering ratio, and bulk refractive index for the entire cruise are provided in **Fig. 10-13**. Final corrected VSF data from MASCOT and LISST sensors are provided in **Fig. 14** for sample casts. Optical scattering from seawater refractive index discontinuities is always present in the LISST near-forward measurements (<~0.1 deg). Vertical profiles of MASCOT scattering are shown in **Fig. 15**. A comparison of total scattering derived from VSF measurements and total scattering from the ac9 showed good agreement (**Fig. 16**). Degree of linear polarization (DOLP) results for 2 casts are shown in **Fig. 17** and are consistent with the previous bench top results of Voss and Fry (1984). The maximum angle of DOLP was typically around 94 deg. (**Fig. 18**). Mie theory results modeling DOLP for bubble populations showed a markedly different function than is typical for particles (**Fig. 19**), with minimal DOLP (i.e., ~0) between 0 and 80 deg. Such a unique DOLP signature could serve as an effective marker for bubbles in-situ. This was testing in SBC with a set of subsurface time series under conditions of actively breaking waves (**Fig. 20**). When healthy bubble populations were present in both horizontal and vertically polarized measurements, results were in reasonable agreement with theory (**Fig. 21**). Another example from the NY Bight with white-capping conditions also shows reasonable agreement with theory (**Fig. 22**). These data underscore the need to switch between polarization states rapidly in-situ (as opposed to consecutive time series of different scattering polarization states), which we are currently working on. We are also working on developing compact, low-power ECO-type sensors for automated platforms to make VSF measurements suitable for discriminating the mid-angle enhancement due to bubbles (**Fig. 23**).

Hawaii. The shape of the mean MASCOT VSF for the entire cruise was typical of previous data (**Fig. 24;** also see **Figs. 27, 28**). Largest standard deviations were located at mid-angles due to the intermittent presence of bubbles at the surface. Mean attenuation and absorption spectra are plotted in **Fig. 25** and are typical for the region. The turbulent component of LISST scattering matched refractive index discontinuities in the water column (**Fig. 26**), consistent with previously reported “schleiren” phenomena (Mikkelsen et al. 2006).

VSF shape in the backward direction was remarkably consistent among the several million MASCOT VSFs collected in 8 field sites exhibiting a wide range in water types (**Figs 27, 28**).

IMPACT/APPLICATIONS

Progress and results represent important steps toward the development and vetting of a multi-angle, in-water VSF device. Knowledge of the Inherent Optical Properties including the VSF can be used to predict and optimize the performance of a host of Naval operations that rely on divers, cameras, laser imaging systems, and active and passive remote sensing systems. These include mine countermeasures, harbor security operations, debris field mapping, anti-submarine warfare, and search and salvage operations.

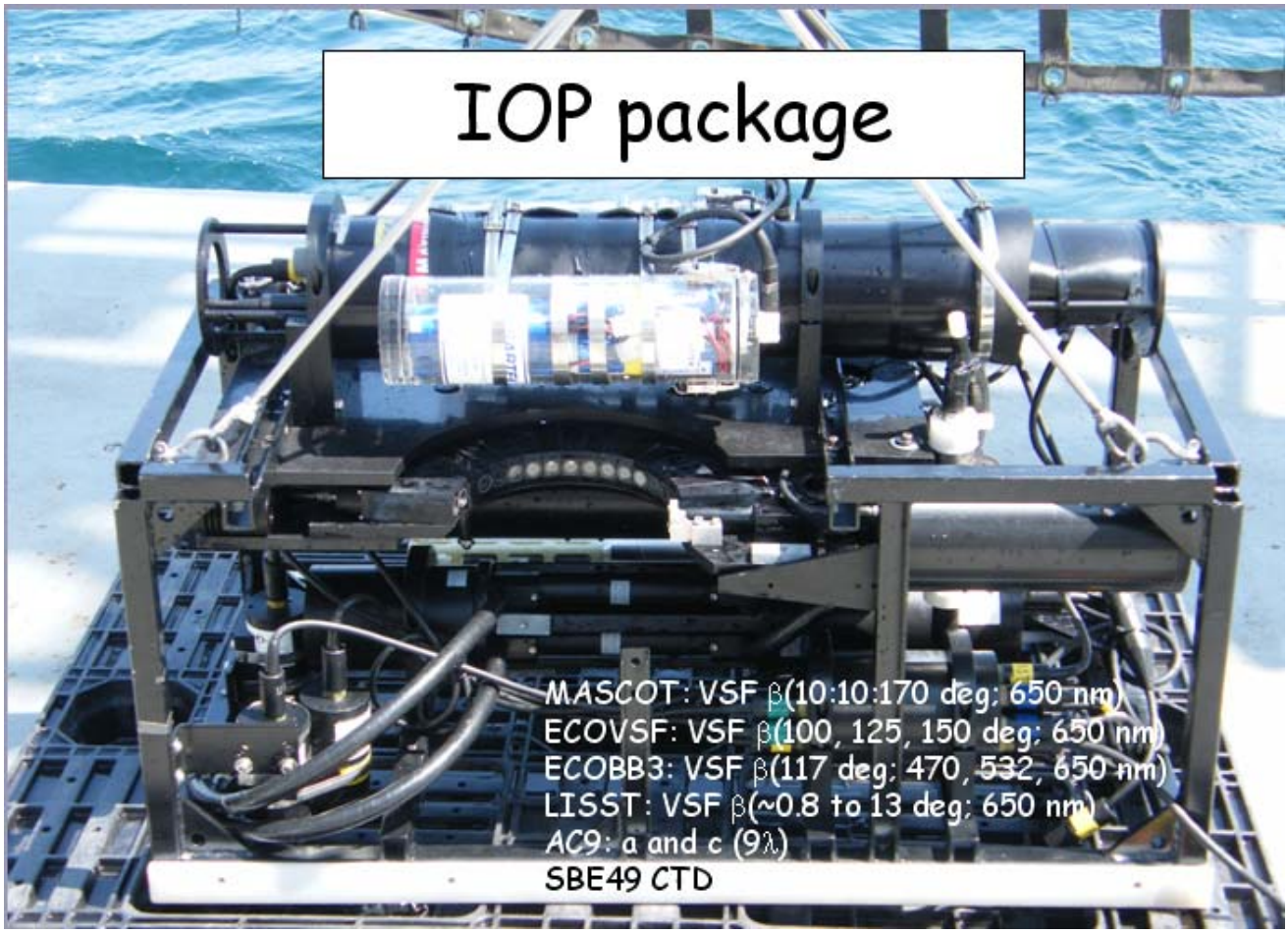

Figure 2. MASCOT VSF device mounted with other optical sensors in a custom cage designed to sample the subsurface domain.

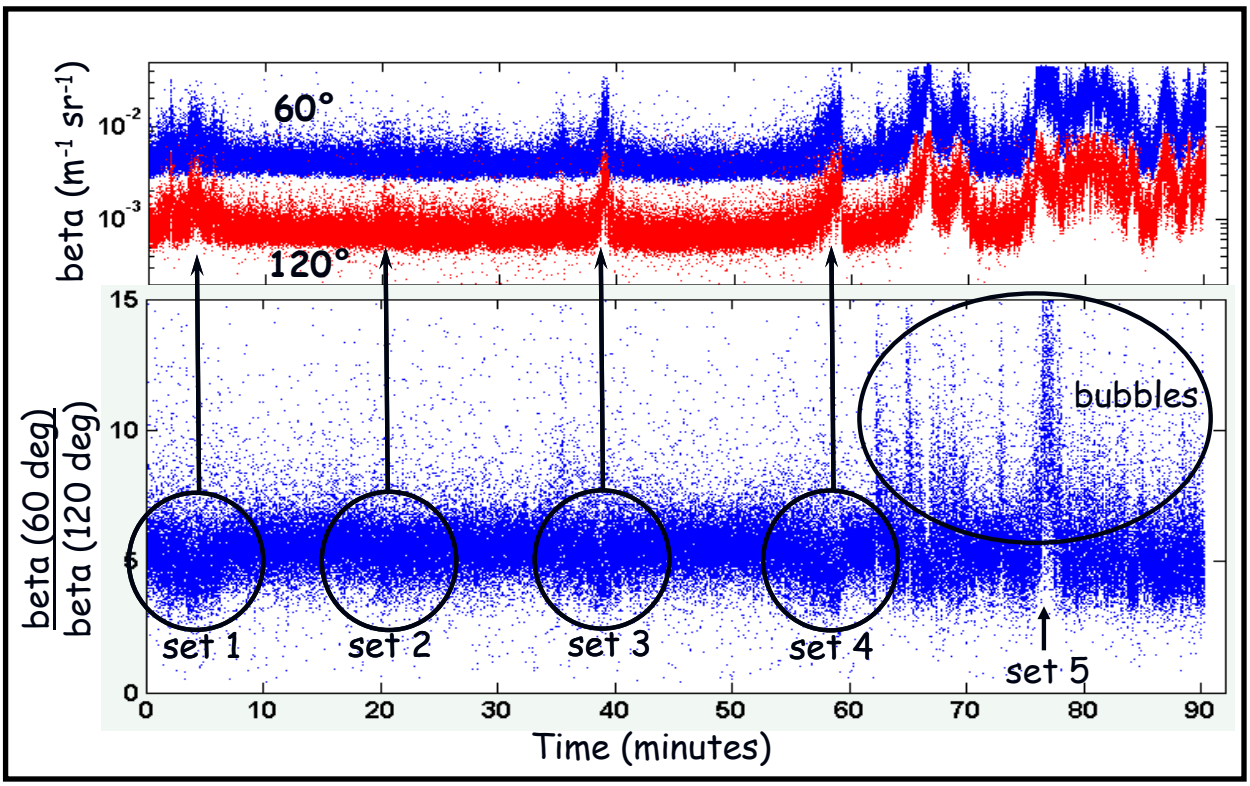

Figure 3. A 90 minute time series of the volume scattering function resolved at 60 and 120 degrees with the MASCOT off Scripps Pier. At the beginning of data collection the surf zone was shoreward of the sensor package and beginning to ebb. Breaking waves generated mixed bubble and sediment plumes which became entrained in a seaward rip current along the pier. By the time these plumes reached the sensor package (tens of seconds), the visible bubble influence had dissipated, leaving the strong sediment contribution. Maximum wave sets broke onshore every ~18 minutes. Scattering plumes from the first 4 sets were dominated by sediment, exhibiting a decreased $\beta(60)/\beta(120)$ relationship due to the sediment dominated plumes having a higher refractive index than the background particle population (e.g., Twardowski et al. 2001). Conversely, when the tide had sufficiently ebbed so that the surf zone was adjacent to the sensor package and active bubble plumes were being directly observed, scattering plumes exhibited an increased $\beta(60)/\beta(120)$ relationship due to the enhancement of mid-angle scattering due to bubbles (e.g., Zhang et al. 2004).

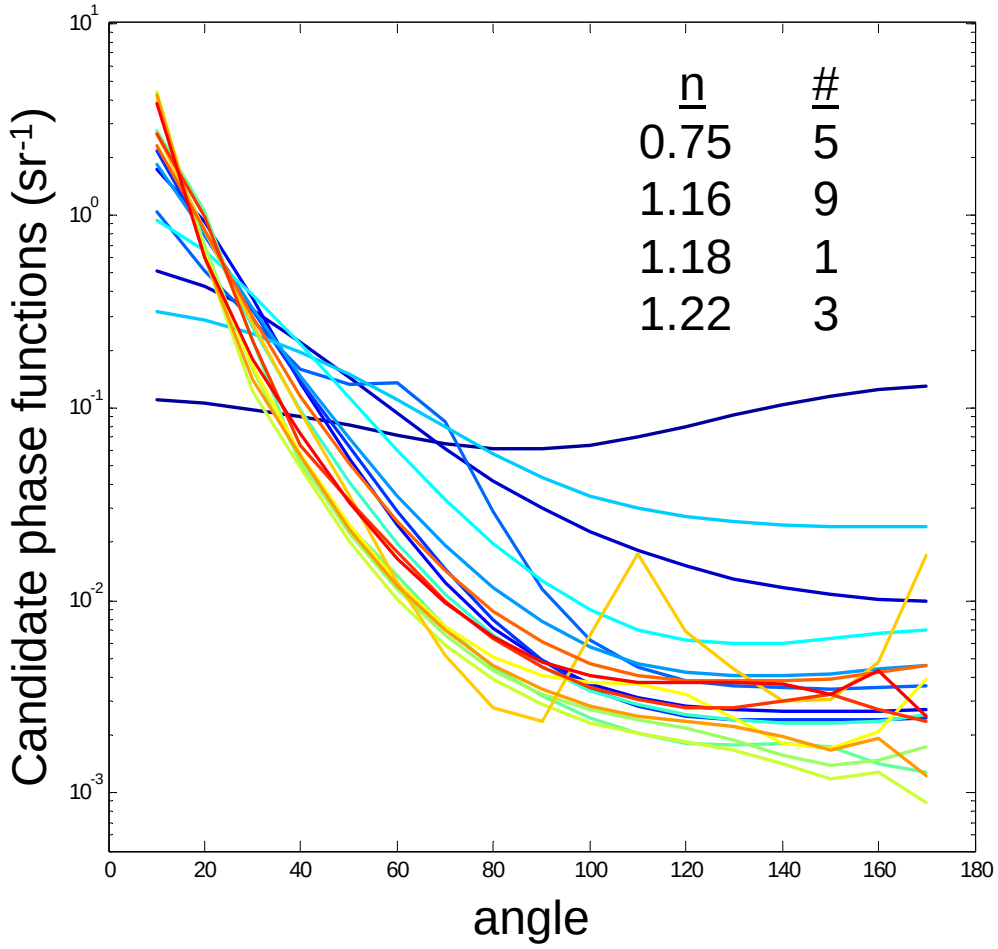

Figure 4. Phase functions computed from Mie theory used in the VSF inversion algorithm. From 180 initial phase functions (particle parameters included 5 bulk refractive indices, 12 modal diameters for a lognormal distribution, 3 standard deviations for the distributions, and a bubble coating thickness scaled at 2%), 59 were determined to be >10% rmse different. After binning the MASCOT VSF time series data from Scripps to 1 Hz (N = 5395), 19 phase functions (plotted here) from the library were picked by the least-squares fitting algorithm to fit these measured VSFs.

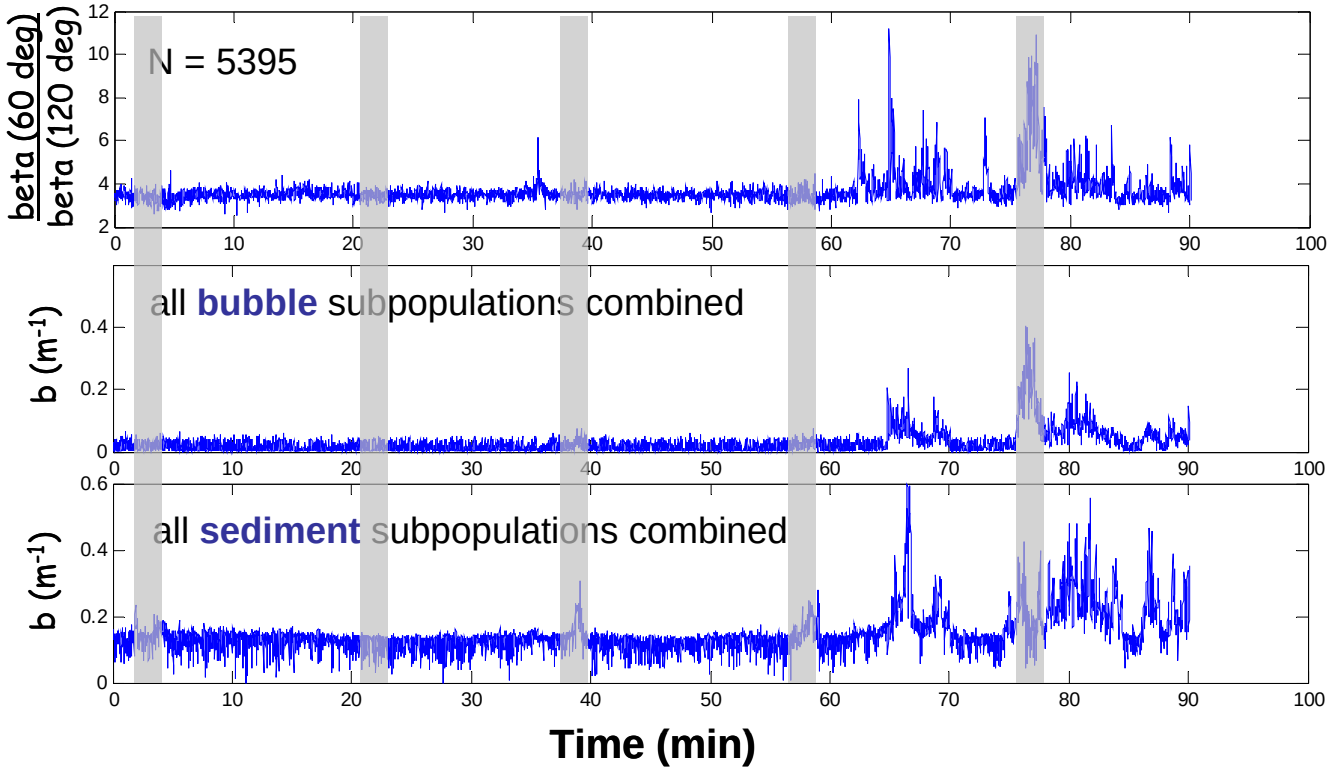

Figure 5. VSF inversion results for the Scripps Pier time series, including panels of β(60)/ β(120) (see Fig. 3), the contribution from all bubble subpopulations to total scattering, and the contribution from all mineral populations to total scattering. The 5 primary wave sets are marked in gray. Results show that increases in scattering during the first 4 wave sets were primarily due to suspended sediments. After the 4th wave set, increases in scattering were due to bubbles and sediments.

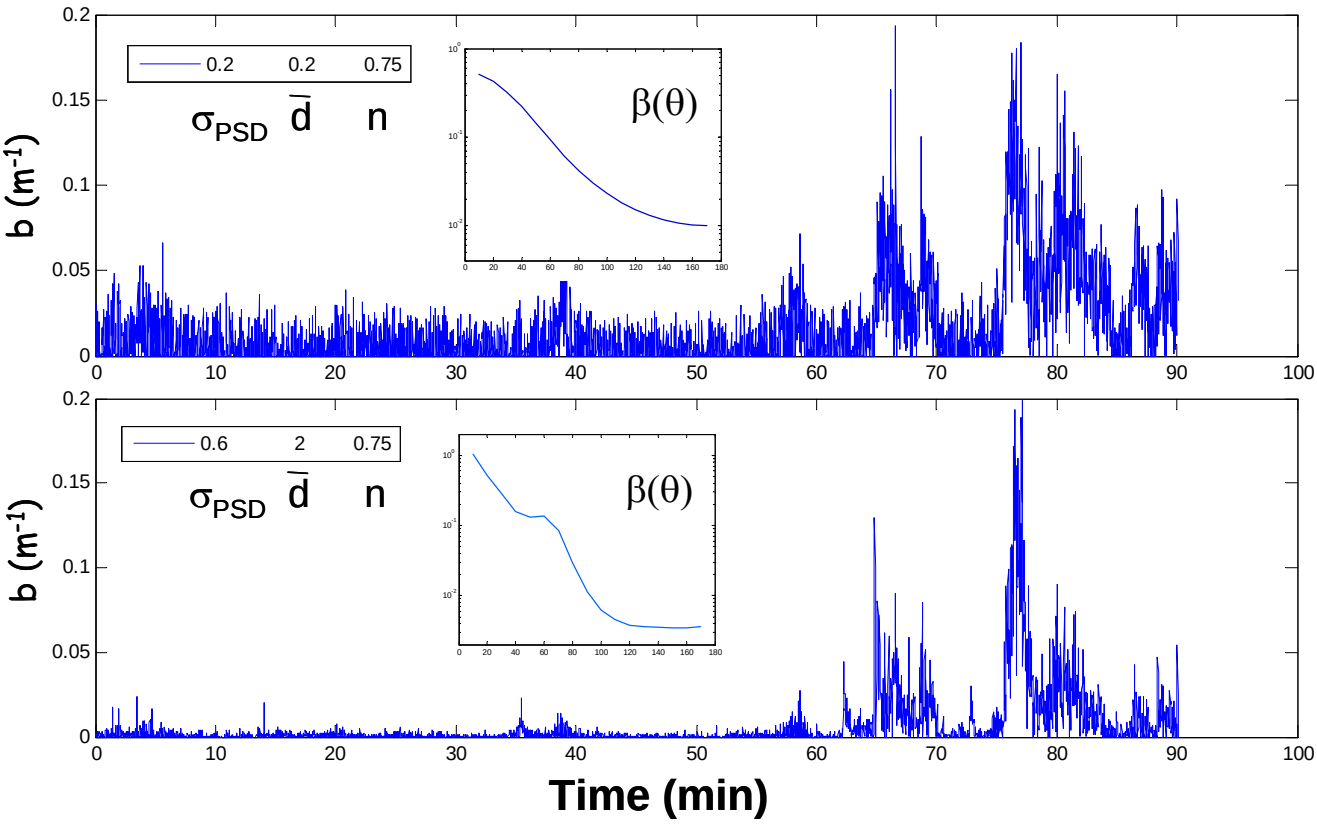

Figure 6. VSF inversion results for the two dominant bubble subpopulations, a small subpopulation with modal diameter and standard deviation of 0.2 μm, and a larger subpopulation with modal diameter and standard deviation of 2 μm and 0.6 μm, respectively. Phase functions of the two subpopulations are shown in the inset of each panel. The mid-angle enhancement due to larger bubbles is evident for the larger bubble population. There is evidence of the small bubble subpopulation in the inversions from the particle maxima observed during the first 4 wave sets. This appears to be evidence of controversial persistent small bubbles (<10 μm) in these "aged" plumes of particles (order of minutes old). Later in the time series when the waves are breaking close to the instrumentation, frequent and substantial peaks in scattering from both small and large bubbles are observed. Some succession can be observed between the large bubble population and the more persistent small bubble population on the order of seconds.

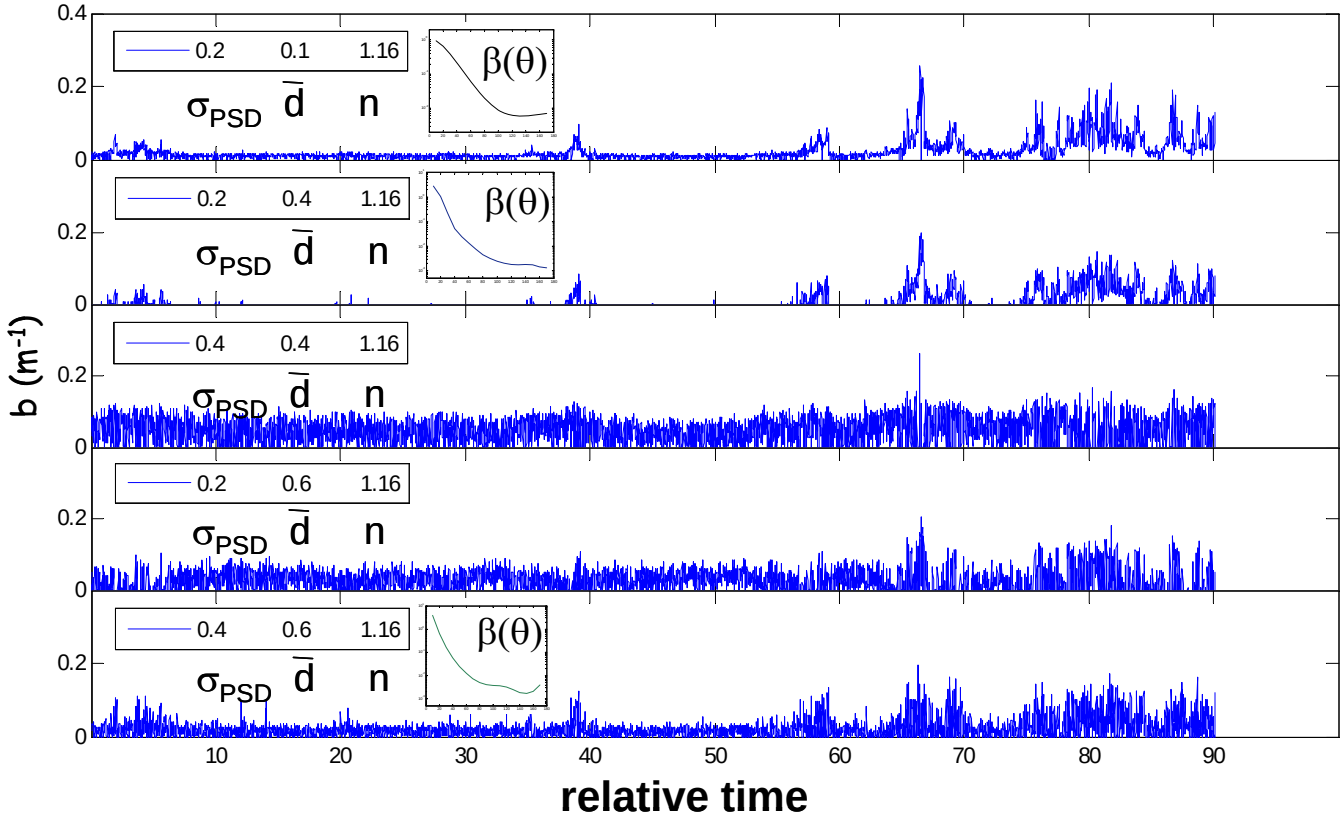

Figure 7. VSF inversion results for the dominant sediment subpopulations, plotted in 5 subpanels, ordered from smallest to largest. Results show the most important sediment subpopulations are the smallest two.

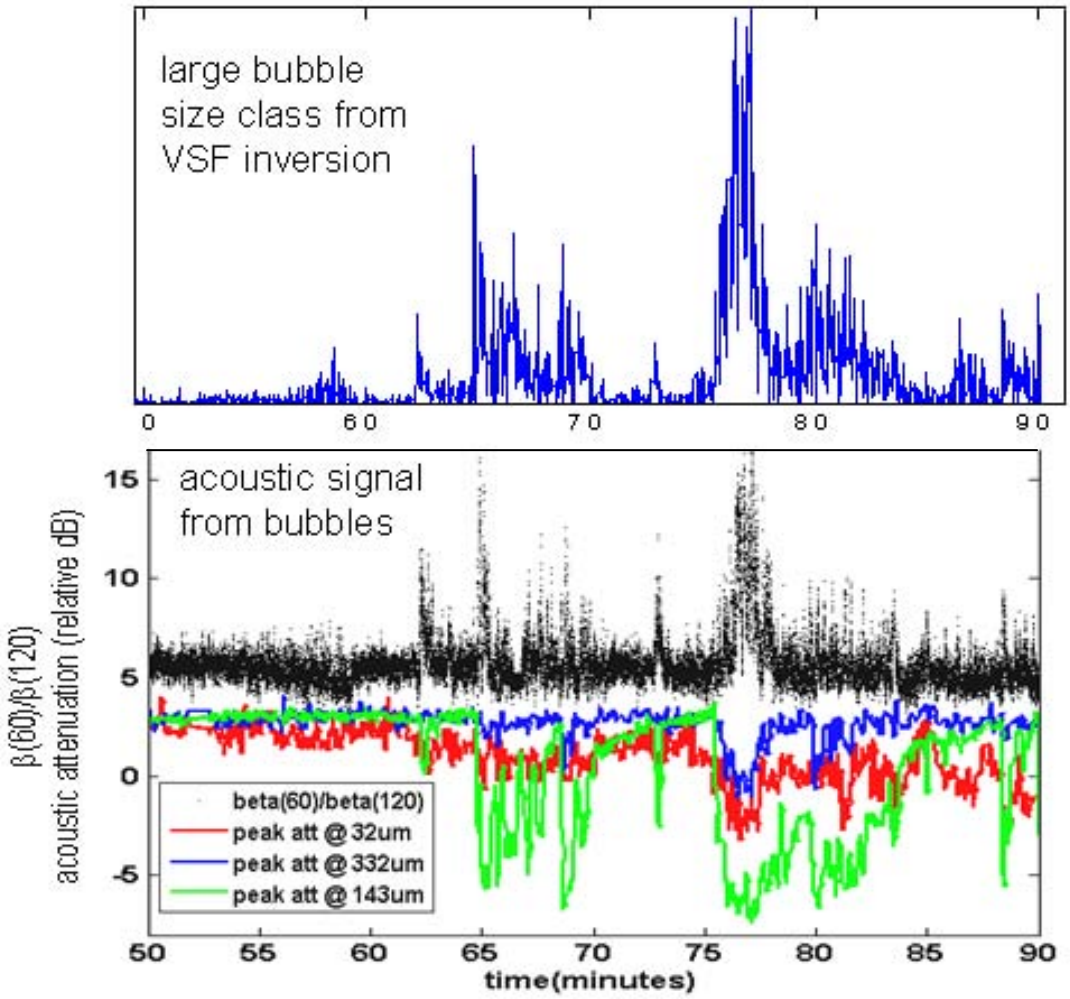

Figure 8. Inversion results from the large bubble population (upper panel) plotted with relative acoustic attenuation from a bubble resonator (lower panel). Patterns were very consistent, more consistent than observed when comparing the acoustic attenuation with positive responses in β(60)/β(120) from the MASCOT (also plotted in lower panel). The response in the simple ratio β(60)/β(120) can get complex when both bubbles and sediment predominate. As a result, on some occasions this ratio disagrees with the acoustic attenuation (e.g., at minute 66.5), whereas the more rigorous VSF inversion results show better agreement. The time series shown here is a subset of the data shown in Fig. 3, including only wave sets 4 and 5. Note that the turbidity maximum observed around 59-60 minutes in Fig. 3 is associated with a decreasing β(60)/β(120), no acoustic response, and only a small response in the large bubble inversion results. This is consistent with the previous interpretation that this turbidity plume is dominated by sediments. A particularly close agreement was observed between the inversion results and acoustic attenuation at the frequency specific for 143um diameter bubbles. Note that even though the two sensors were on the same instrument package, sample volumes were separated by about 60 to 70 cm.

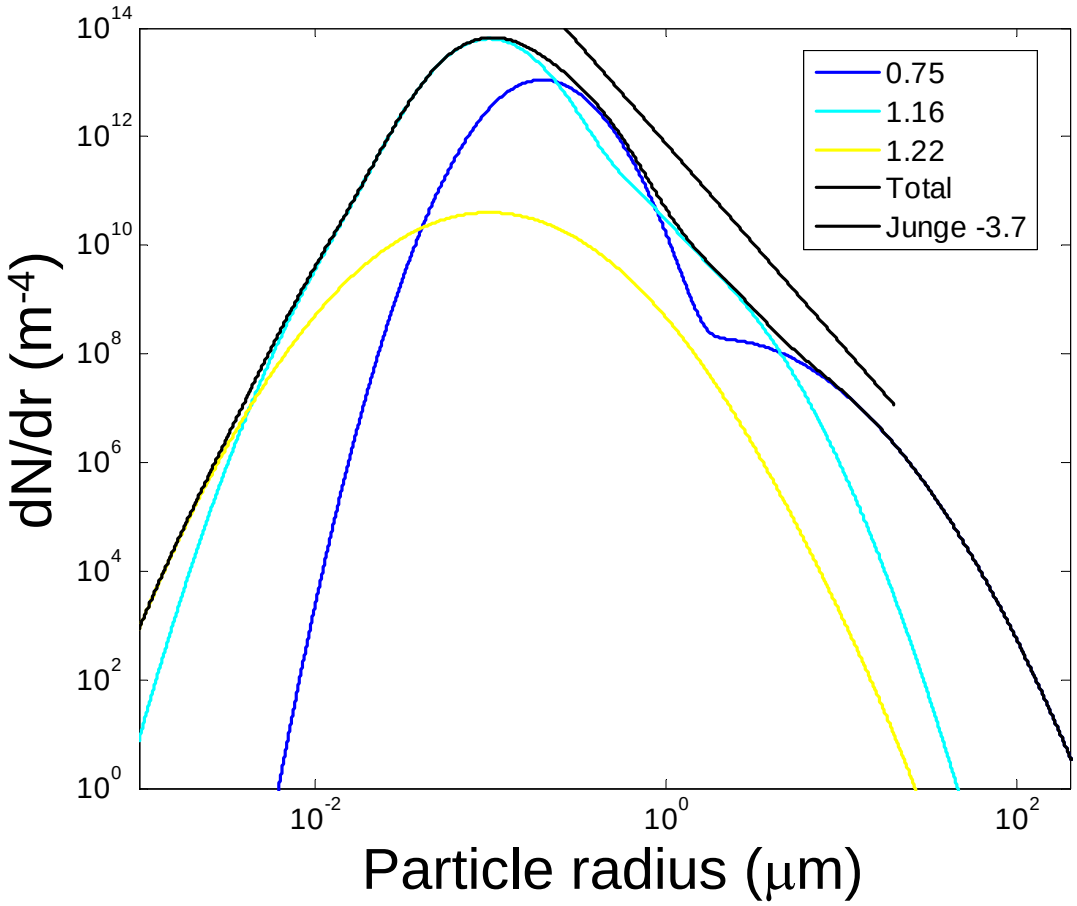

Figure 9. Size distributions of dominant subpopulations with relative refractive indices of 0.75 (bubbles), 1.16 (quartz-like minerals), and 1.22 (clay-like minerals). The aggregate size distribution (in black) is modeled well with a hyperbolic differential Junge-type model with slope 3.7 in the range that can be resolved by sizing devices such as a coulter counter. Many previous studies looking at oceanic size distributions have observed that the Junge distribution is a good model, which serves as an element of validation for our inversion results.

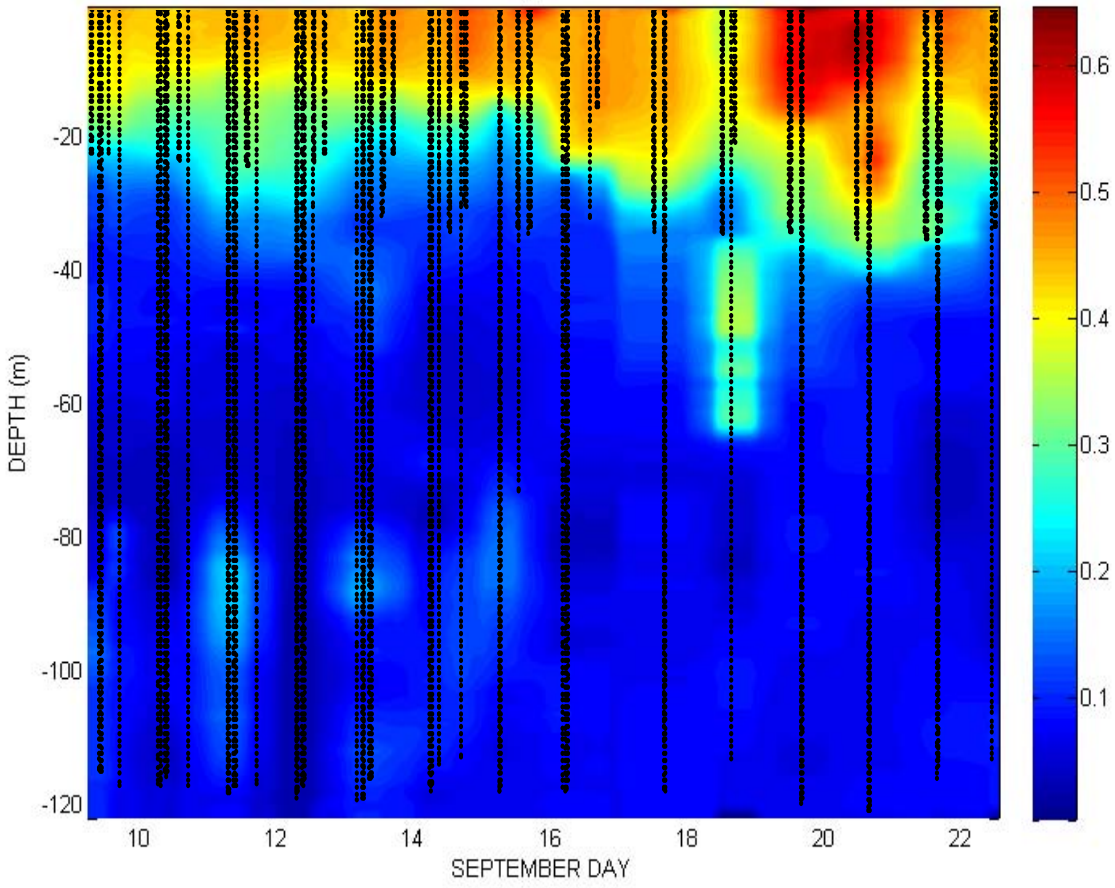

Figure 10. Non-water beam attenuation coefficient at 650 nm, cpg(650), from Santa Barbara Channel 2008.

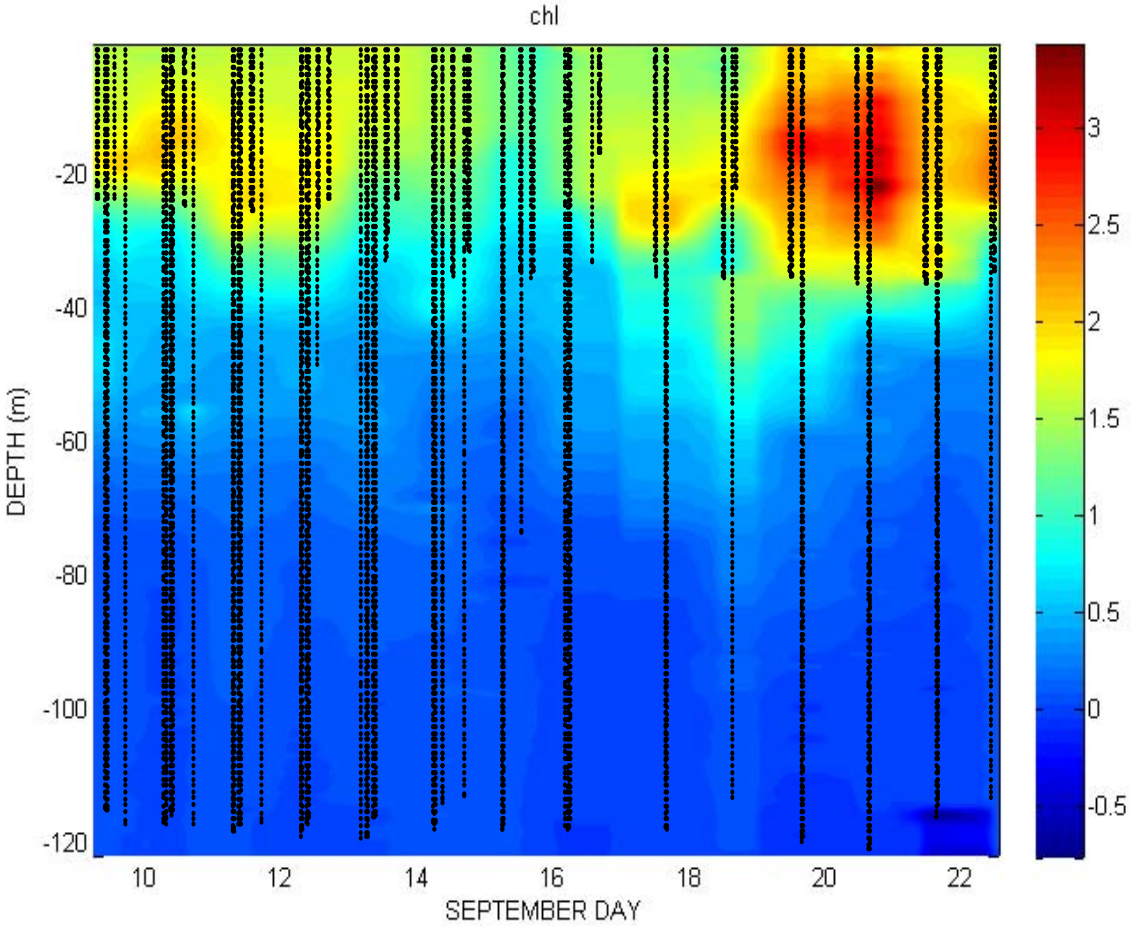

Figure 11. ac-9 derived chlorophyll from Santa Barbara Channel 2008.

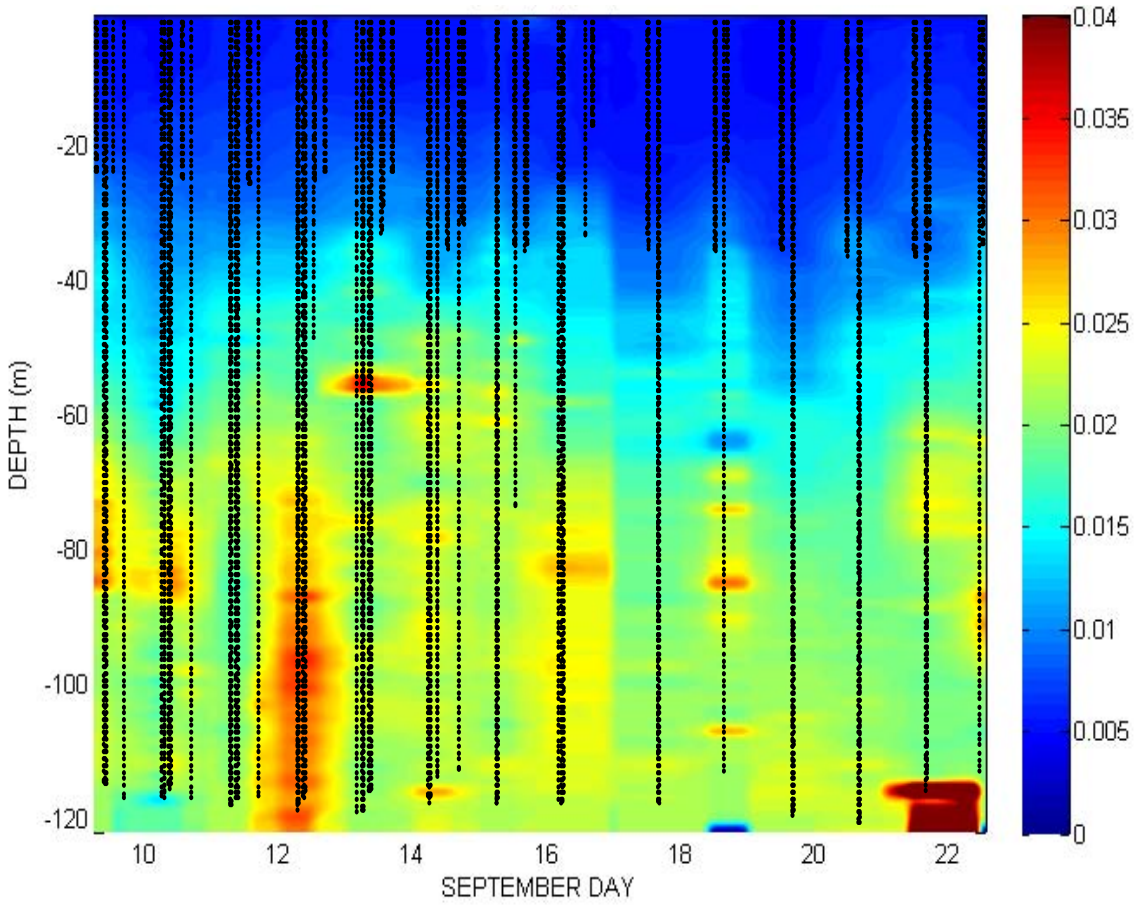

Figure 12. Backscattering ratio at 657 nm, bbp(657)/bp(657), from Santa Barbara Channel 2008.

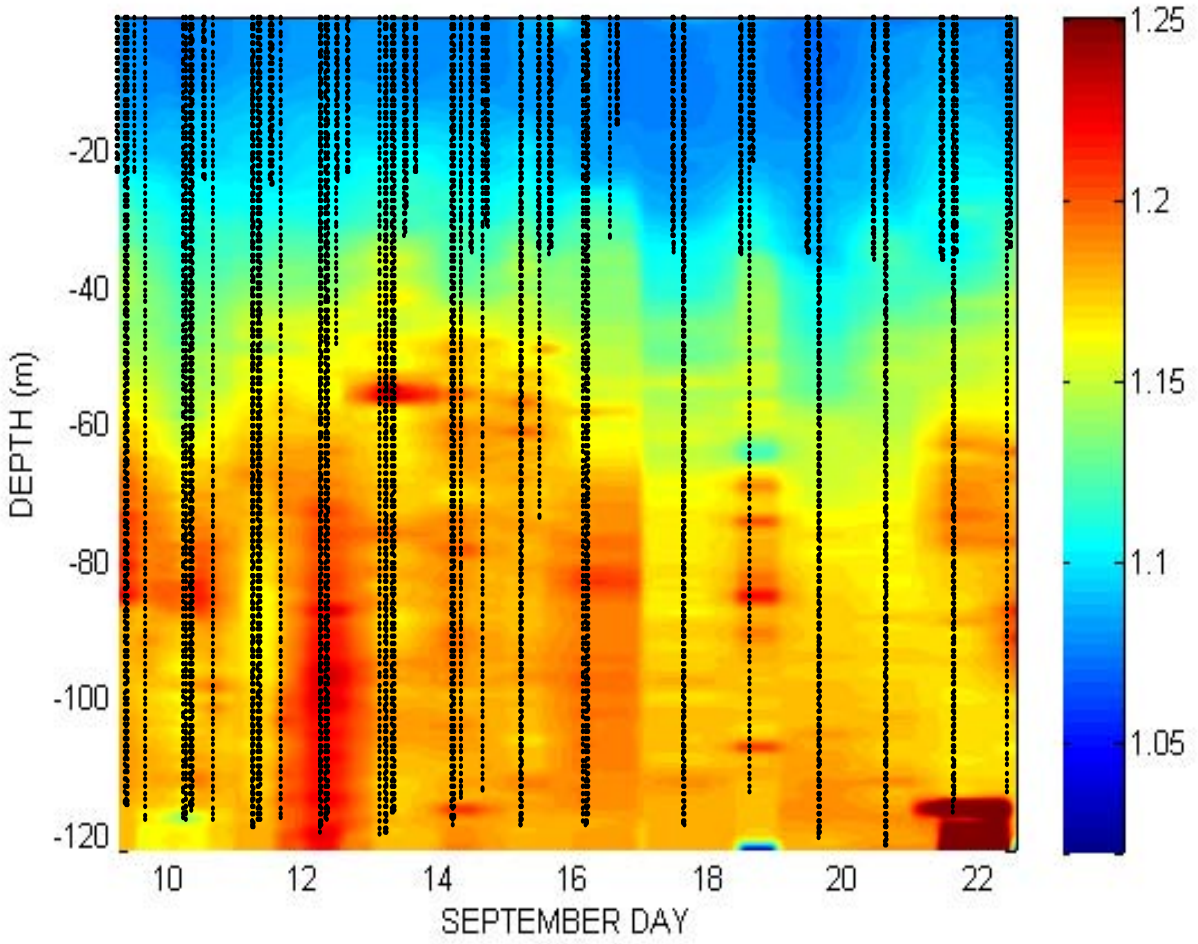

Figure 13. The bulk refractive index estimated according to Twardowski et al. (2001) from Santa Barbara Channel 2008.

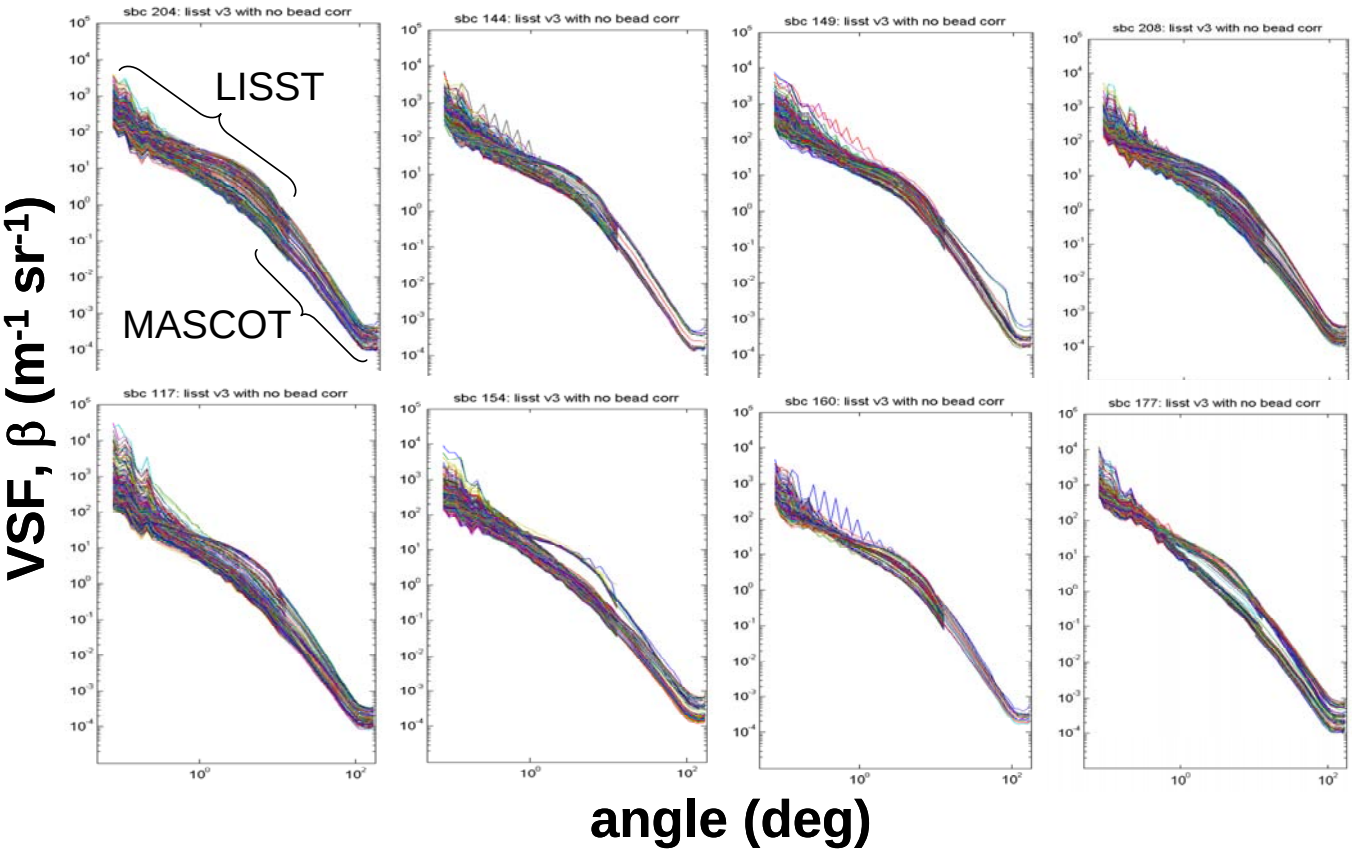

Figure 14. Example VSFs plotted as a function of angle from 120 m vertical profiles collected with MASCOT and LISST sensors in SBC. Agreement between MASCOT and LISST sensors in the region of overlap (around 10 deg) is excellent. Sensor calibrations are completely independent. Optical scattering from turbulent refractive index discontinuities is present in all near-forward LISST data (less than ~0.1 deg). In some casts such as SBC 149, a mid-angle enhancement due to bubbles can be observed in some (subsurface) VSFs.

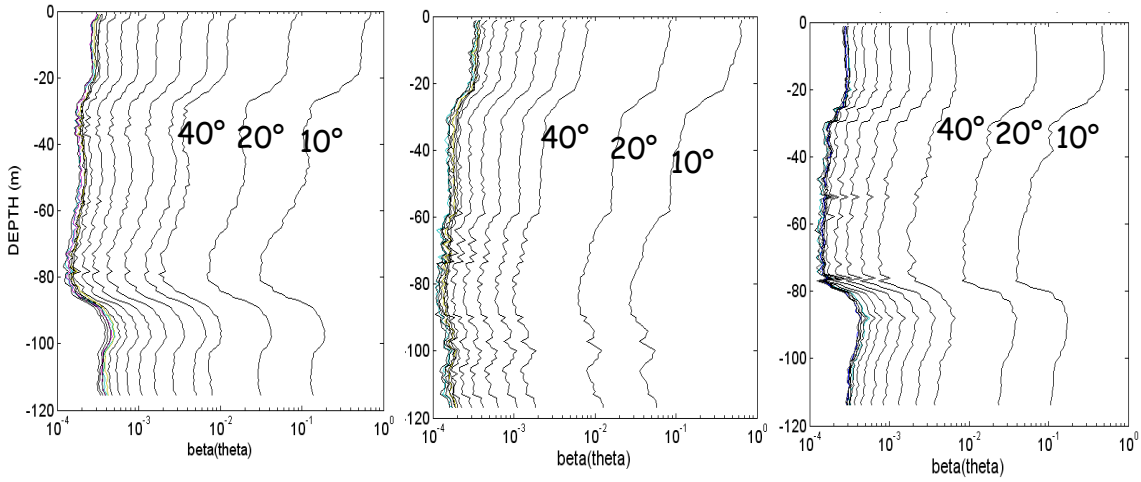

Figure 15. MASCOT VSF data plotted as function of depth for all 17 angles except 30 deg (faulty detector). A surface particle maximum was always present. A deep maximum of resuspended sediments was sometimes present. The clearest water was observed around 80 m.

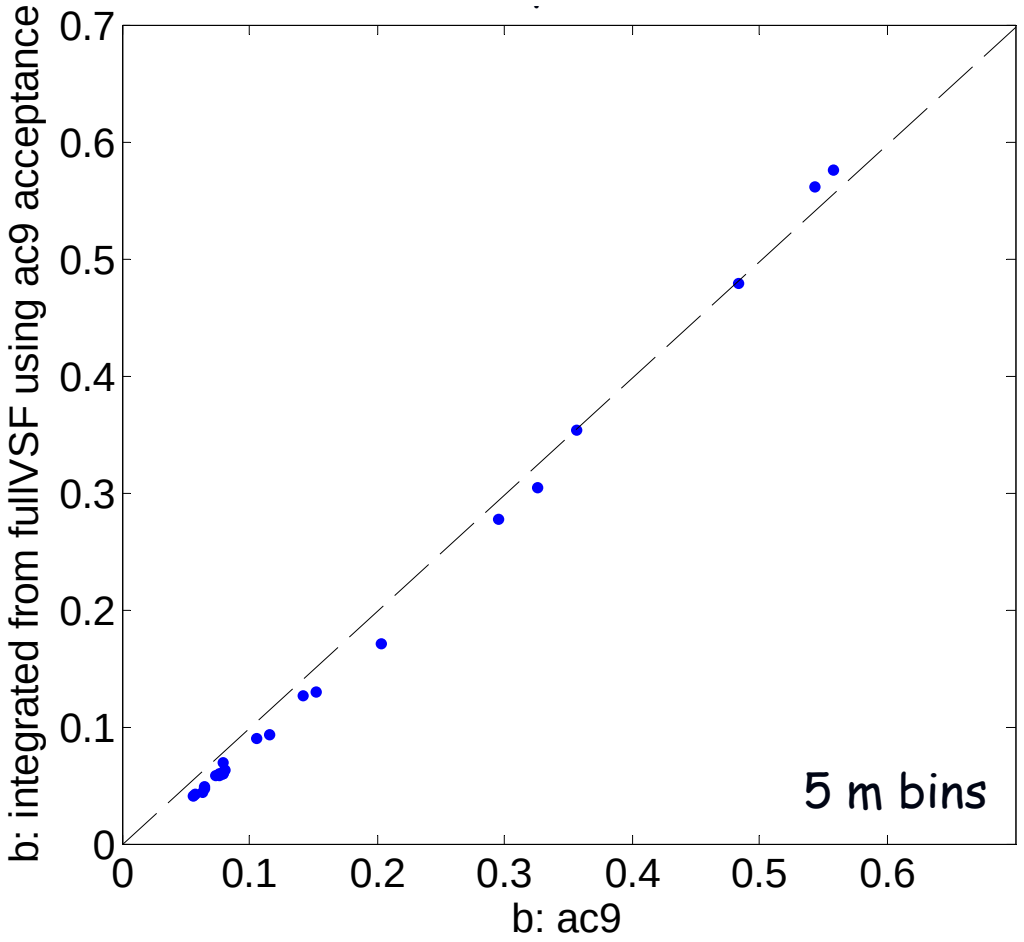

Figure 16. Good agreement was observed between total particle scattering derived from integrating the full volume scattering function using the acceptance angle of the ac9 (0.93 deg) as the minimum angle and total particle scattering measured with an ac9. These data are from one 120 m cast on Sept. day 19.69.

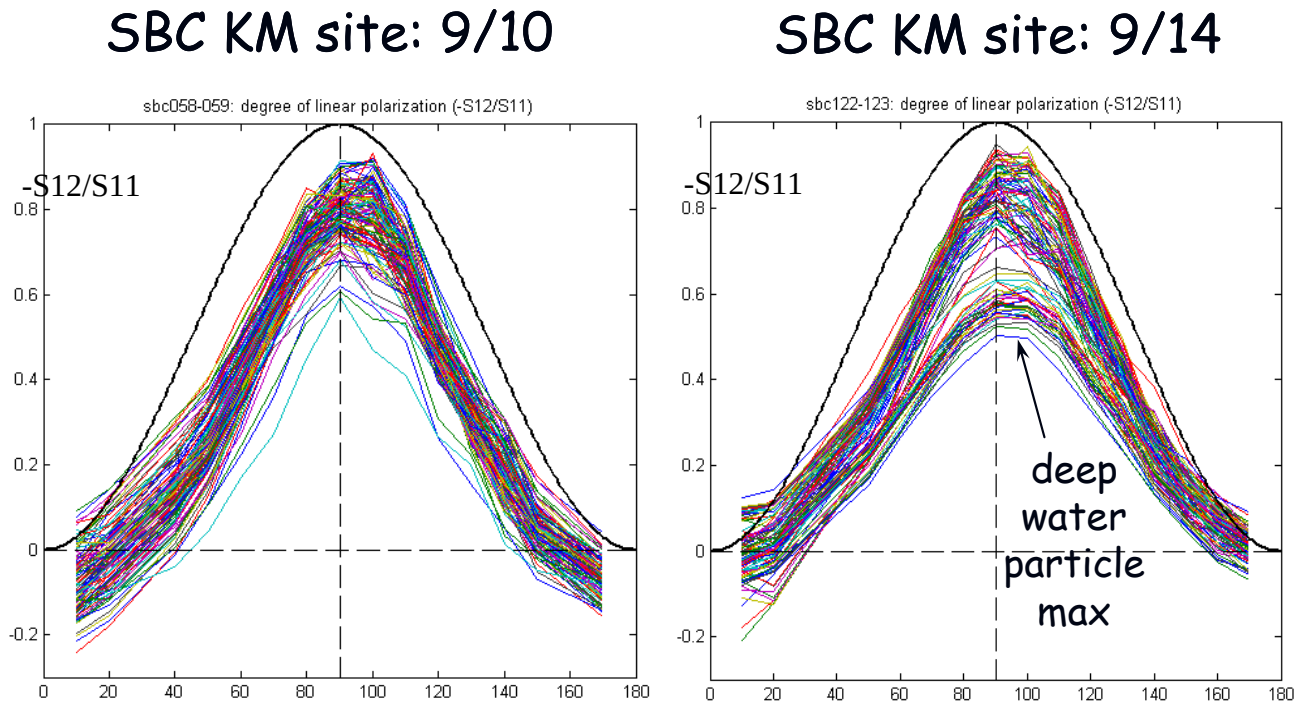

Figure 17. MASCOT degree of linear polarization (DOLP) as a function of angle for 2 example profiles, the second of which sampled a deep water particle maximum comprised of resuspended sediments (with corresponding minimum in DOLP). Shapes are generally consistent with Voss and Fry (1984), where maxima typically occur around 0.8 and at angles just larger than 90 deg; near 0 and 180 DOLP converges on zero.

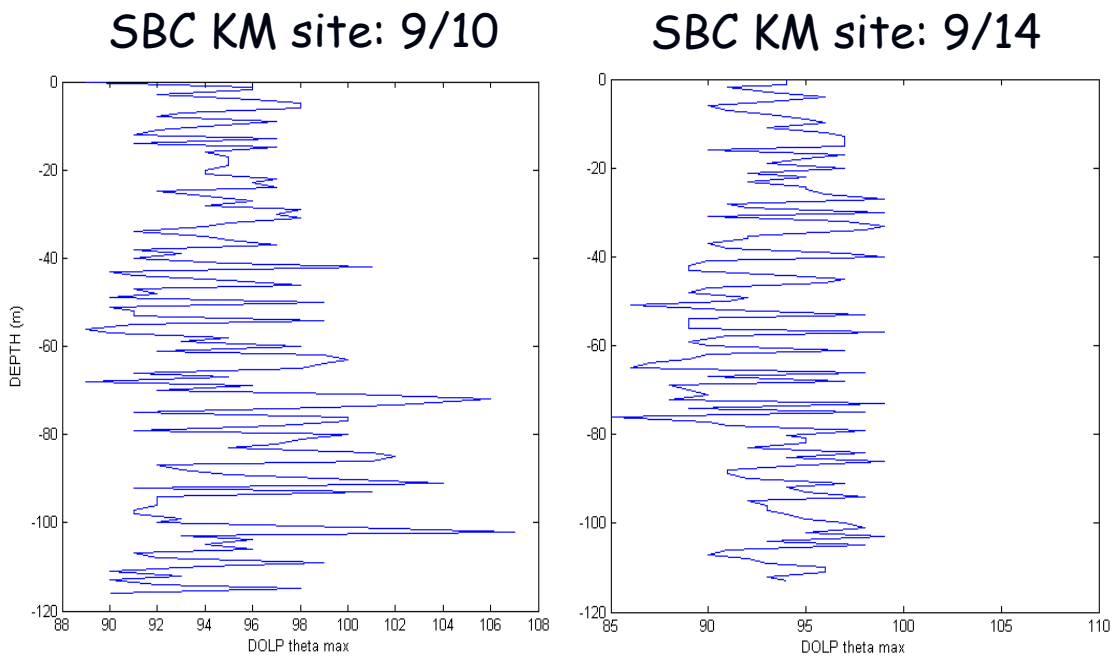

Figure 18. Angles for MASCOT DOLP maxima for the profiles from Fig. 17, estimated with a cubic spline fitting algorithm.

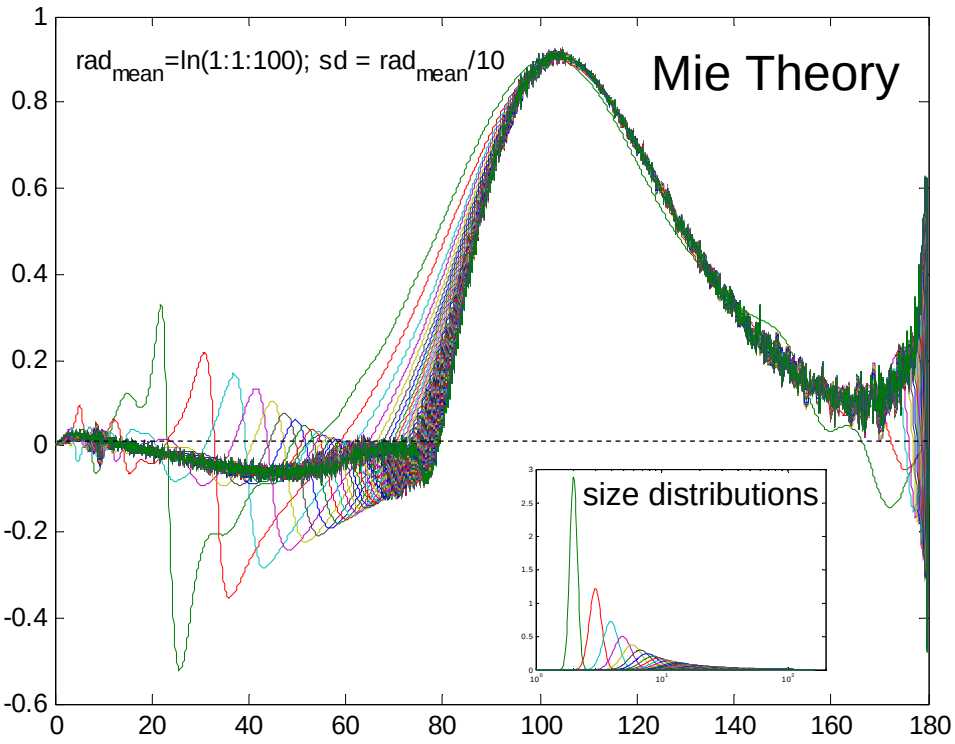

Figure 19. Theoretically derived DOLP for lognormally-distributed bubble populations. The mean radius varied according to ln(1:1:100) and the standard deviation for the distribution varied according to 10% of the mean radius. Size distributions are plotted in inset graph. Results show that DOLP for bubble populations can be expected to be very different in shape than DOLP for oceanic particles (e.g., see Fig 17).

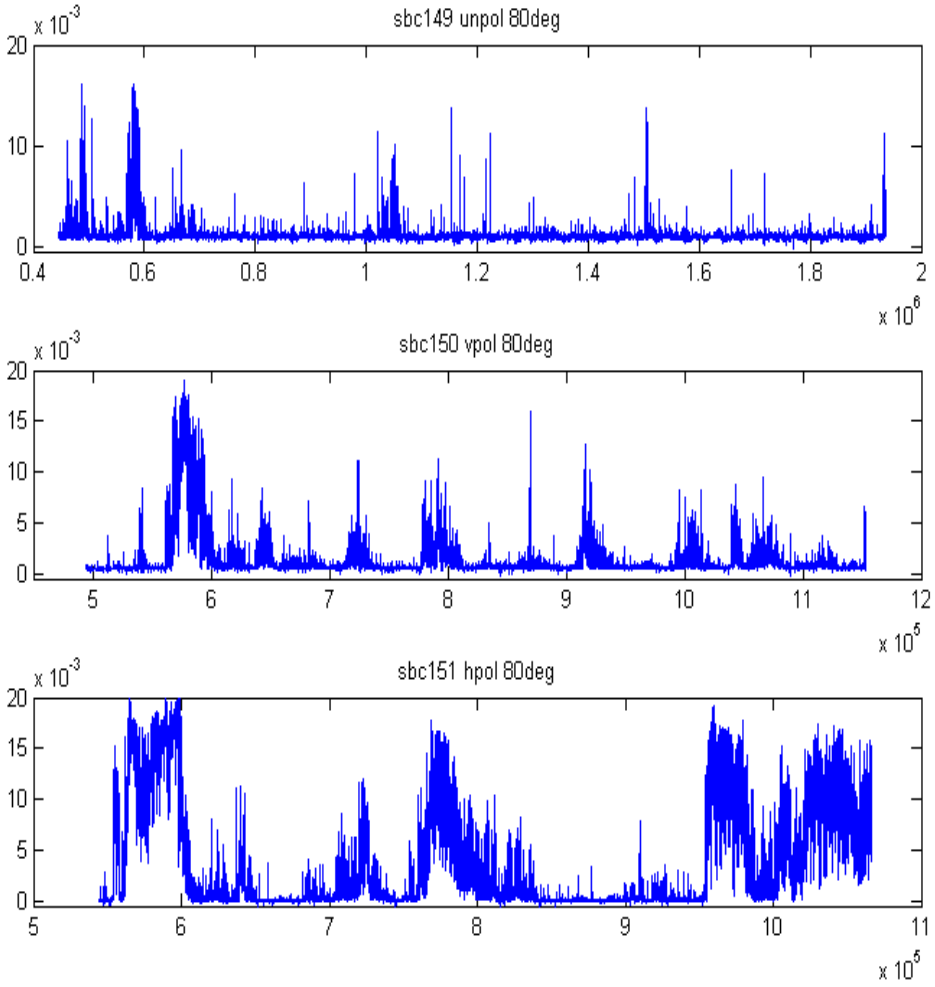

Figure 20. Subsurface time series of MASCOT VSF scattering at 80 deg. (location of mid-angle enhancement due to bubbles) for an unpolarized source (top panel), a vertically polarized source (middle panel), and a horizontally polarized source (bottom panel). Time series were collected consecutively, requiring retrieval of the instrument package and manual polarization switching between each series. Data was collected during 20-25 knt winds accompanied by extensive white capping. All observed enhancement above the baseline in each time series is due to injected bubble particle fields.

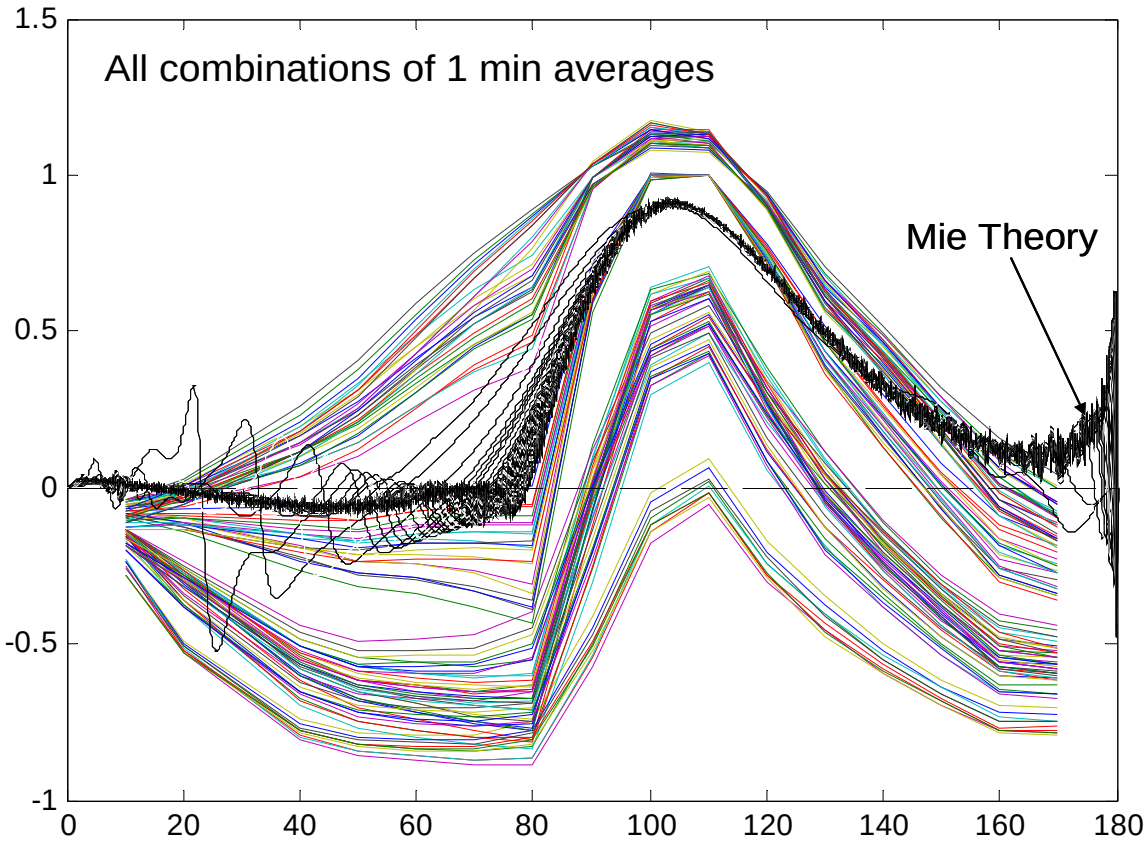

Figure 21. DOLP computed from all combinations of 1 minute time averages from the time series plotted in Fig. 20. In cases where healthy bubbles are observed in both the vertically and horizontally polarized source measurements, the resulting DOLP showed reasonable agreement with the theoretical expectation. For those cases where bubbles were in low abundances, the resulting DOLP showed a more typical shape consistent with background particles (e.g., see Fig. 17). For those cases where bubbles were moderate abundance relative to background particles, a DOLP in between these DOLPs was observed. However, when healthy bubbles were observed in one polarization measurement and not the other, unrealistic, strongly negative DOLPs were observed.

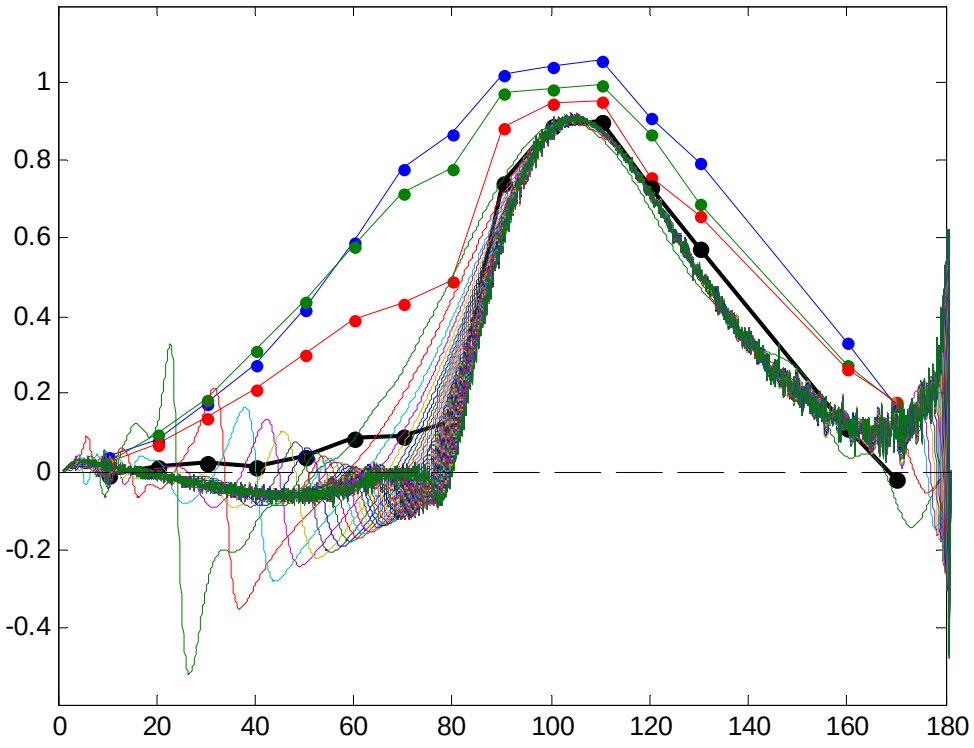

Figure 22. DOLP results observed in NY Bight under extensive whitecapping. Again, reasonable agreement between measurement and theoretical expectation is observed.

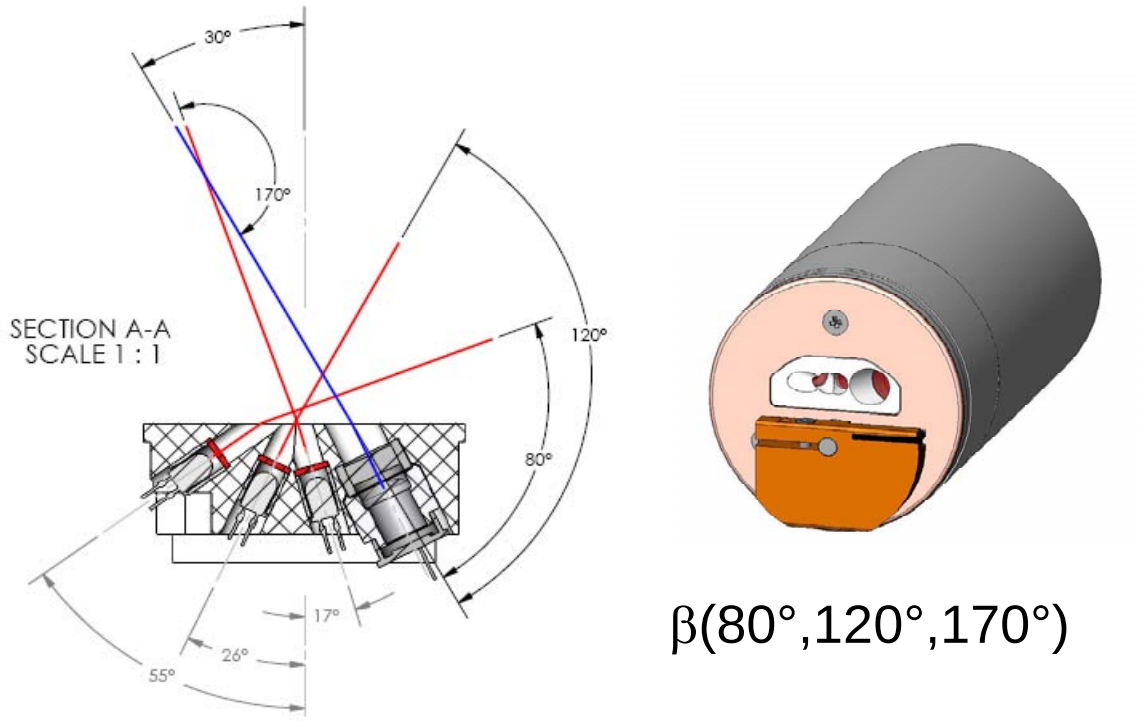

Figure 23. Newly developed low power, compact ECO-type sensor for discriminating the mid-angle scattering enhancement characteristic of bubbles greater than a several μm in diameter. Sensor is suitable for deployment on compact autonomous platforms.

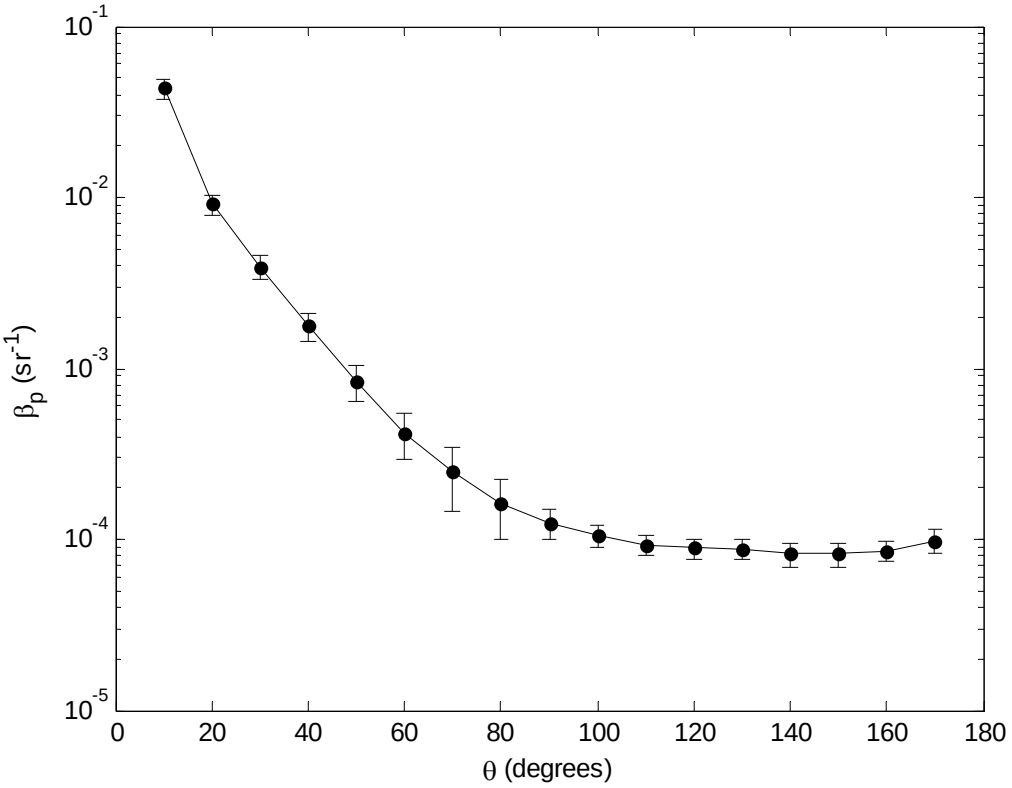

Figure 24. Mean and standard deviation of MASCOT non-seawater VSF for Hawaii cruise AUG-SEP 2009. Note largest standard deviations are associated with middle angles where intermittent bubbles exhibit enhanced scattering.

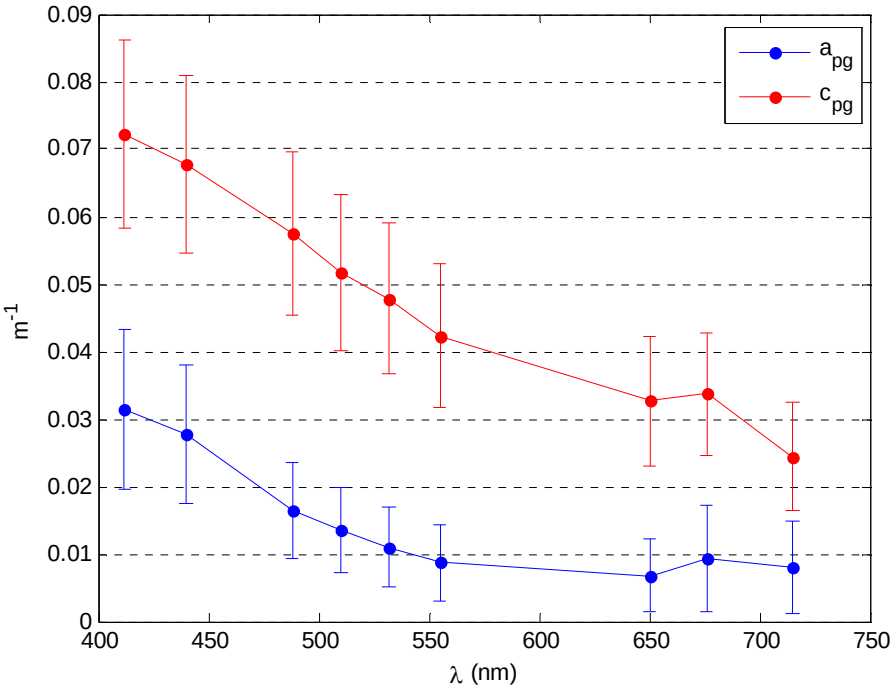

Figure 25. Mean non-seawater attenuation (c_{pg}) and absorption (a_{pg}) spectra for Hawaii cruise AUG-SEP 2009.

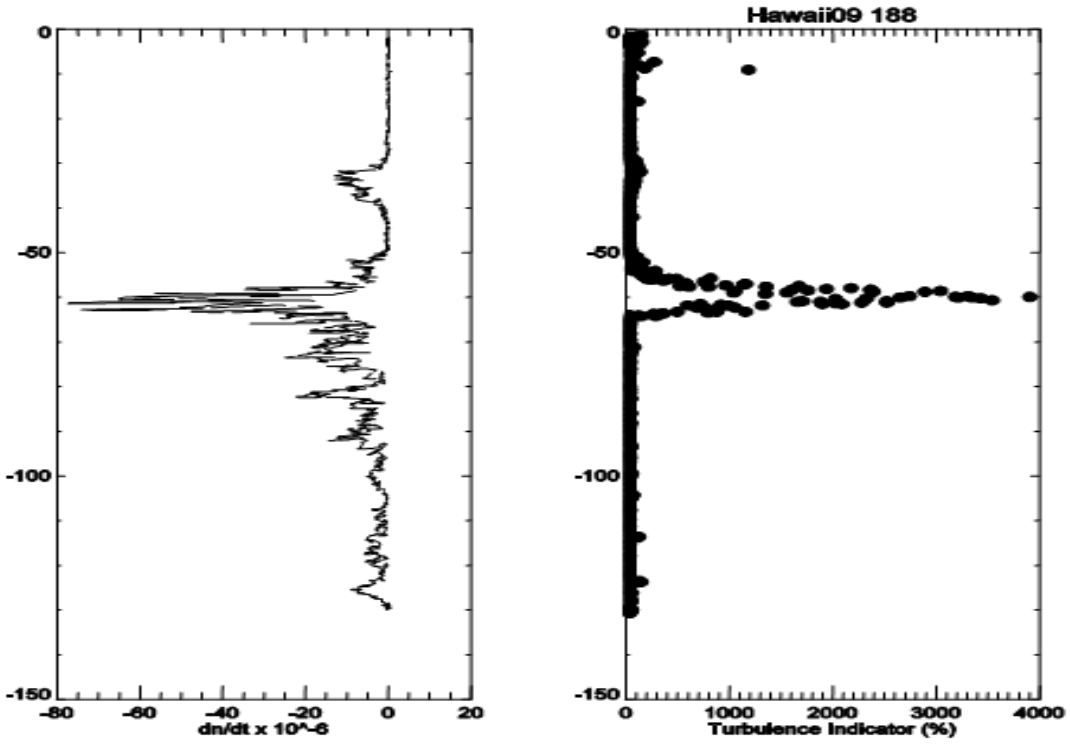

Figure 26. Seawater refractive index gradient as a function of depth and optical turbulent scattering in the near-forward measured with the LISST. A strong gradient in refractive index is observed around 60 m with a concomitant increase in turbulent scattering derived from the LISST data.

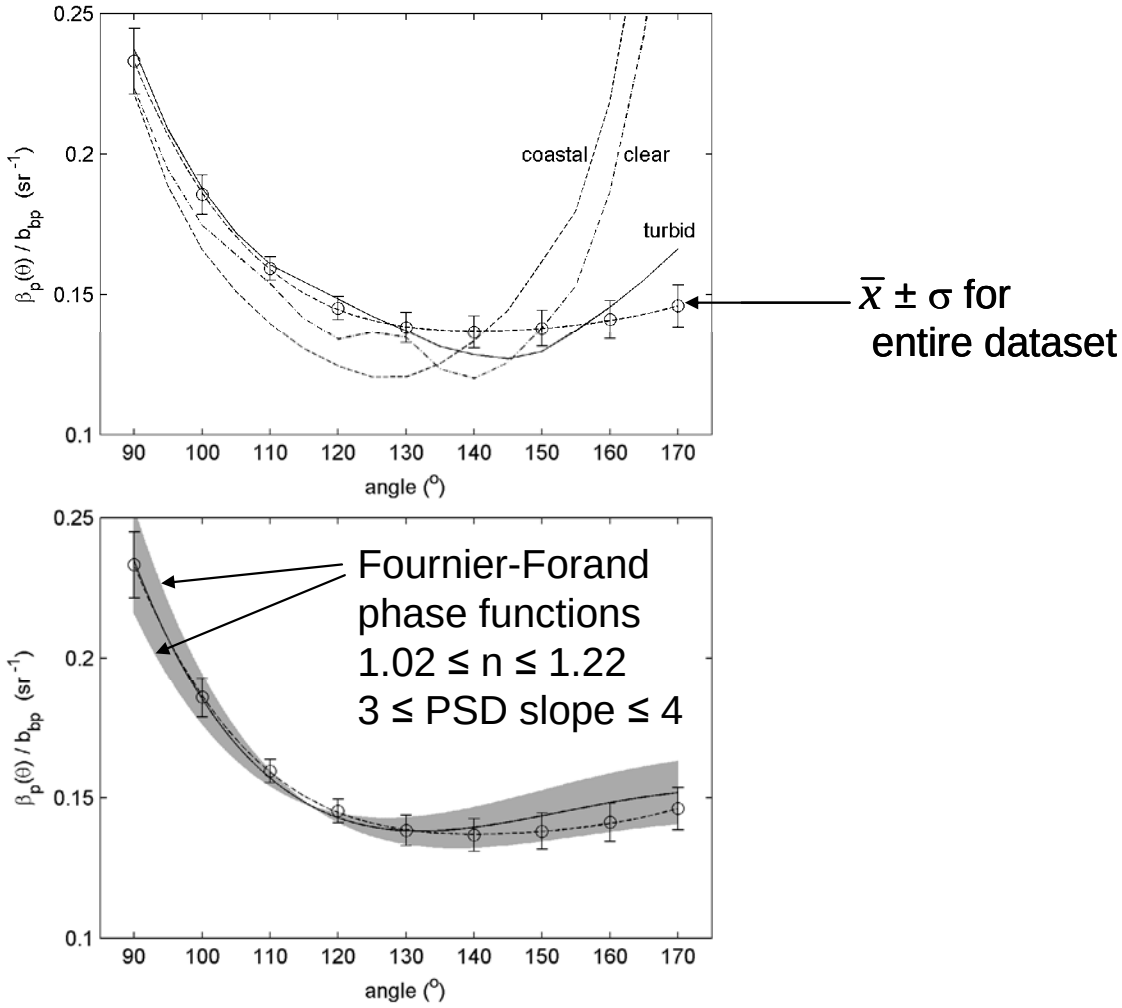

Figure 27. Mean and standard deviation of MASCOT phase function data in the backward direction for several million VSFs collected during field exercises in 8 sites ranging widely in water type from clear waters off Hawaii and in the Ligurian Sea to turbid waters of NY Harbor (circles with dashed line in upper panel). The coastal, clear, and turbid water phase function data of Petzold (1972) are also plotted in the upper panel, with the turbid measurement showing the best agreement. The smallest standard deviation in phase function was observed at 110 and 120 deg. Fournier-Forand phase functions exhibit a similar shape to our averaged phase function in the backward and also show smallest deviation between 110 and 120 deg.

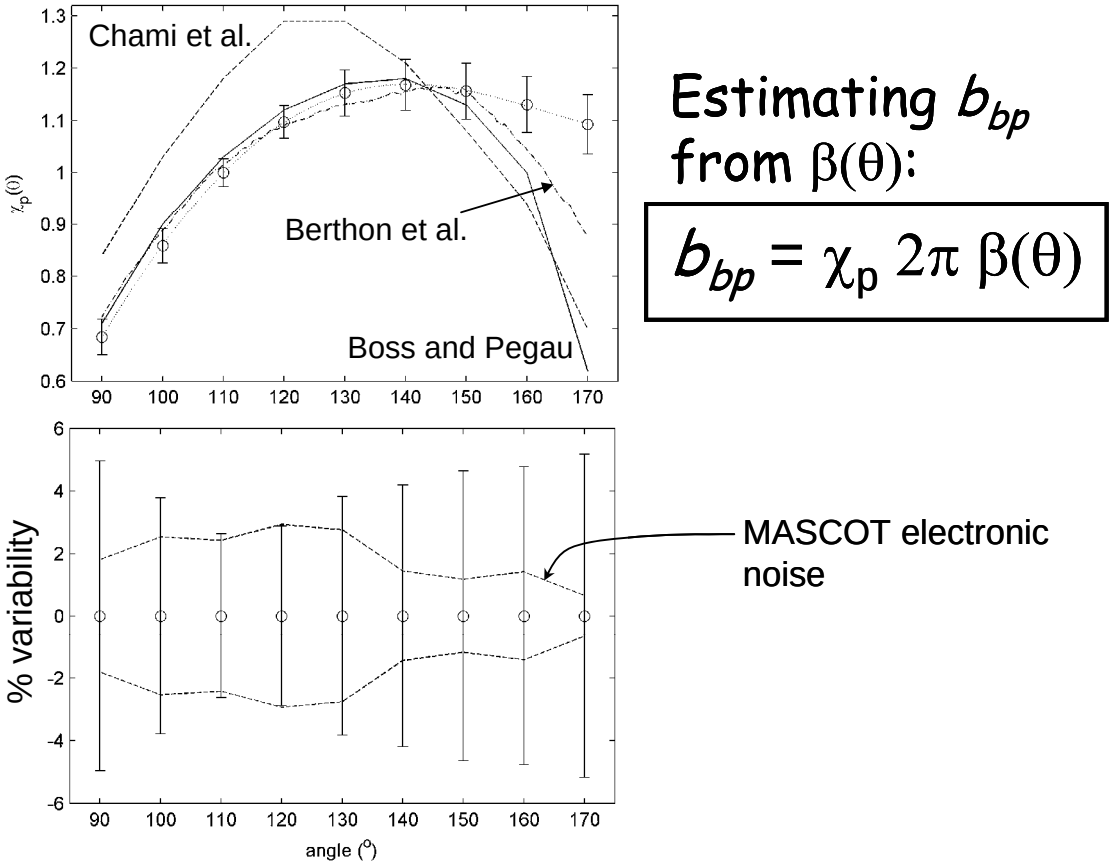

Figure 28. The factor χ is used to convert a VSF measurement, β, to a backscattering coefficient according to $b_{bp} = \chi_\pi\, 2\pi\, \beta_\pi(\theta)$, and is most effective at the angle where the backward phase function shows the smallest variability in an extensive data set. The χ as a function of angle is plotted for our data set in the upper panel along with previous results from isolated regions collected with a Ukrainian device called the MVSM (Boss and Pegau 2001; Berthon et al. 2007; and Chami et al. 2005). Our results agree reasonably well with previous results except for Chami et al. MVSM results in general exhibit lower χ values in the near-backward, perhaps consistent with a reflection problem, which is always a challenge for these types of measurements. The lower panel shows the %variability for our phase function data along with the MASCOT electronic noise estimated from in-situ dark count measurements. Remarkably, the baseline noise is comparable to the ~2% variability observed the phase function around 110 and 120 degrees, indicating that almost all the variability observed is instrument noise and the subsequent "real" variability in the phase function at these angles is practically negligible.

TRANSITIONS

We expect that our efforts in developing an in-water VSF device and associated inversion techniques to better understand particle dynamics in natural waters will lead to transition as operational tools for the fleet and the oceanographic research community in the future.

RELATED PROJECTS

This effort is related to several ongoing efforts by the PI to develop optical sensors and associated biogeochemical inversion techniques to improve our understanding of the oceanic environment. Current ongoing related projects include:

- investigating the dynamics of scattering by subsurface bubble populations and other particles in the S. Ocean (NASA, Twardowski; project lead PI H. Dierssen);
- investigating the underlying controls of biological camouflage responses in dynamic underwater optical environments (MURI collaboration, Twardowski; URI PIs J. Sullivan and B. Seibel; project lead PI M. Cummings);
- developing improved remote sensing water quality algorithms for coastal waters (NASA, Twardowski; project lead PI Z-P. Lee);
- developing compact, low power sensing tools for ocean observing platforms (ONR SBIR, Twardowski);
- developing a microscopic holographic camera for optically relevant particles (NOPP, project lead PI J. Sullivan);
- developing optical prediction models for the surfzone (CEROS, Twardowski; project lead PI G. Chang); and
- developing a surfzone drifter measuring optical attenuation and scattering (ONR SBIR, Twardowski).

PUBLICATIONS

Twardowski, M.S., J.M. Sullivan, P.L. Donaghay, and J.R.V. Zaneveld. 1999. Microscale quantification of the absorption by dissolved and particulate material in coastal waters with an ac-9. *J. Atmos. Ocean. Technol.* **16(12**):691-707. [refereed]

Boss, E., and M.S. **Twardowski**. 2000. On the relationship of the particulate beam attenuation spectrum and size distribution of oceanic particles. *Proceedings from Ocean Optics XV*, October 16-20, Monaco.

Coleman, J.E., R.A. Reynolds, M.C. Talbot, M.S. **Twardowski**, M.J. Perry. 2000. Utilization of solar-induced chlorophyll a fluorescence as an indicator of phytoplankton biomass in coastal waters. *Proceedings from Ocean Optics XV*, October 16-20, Monaco.

Eisner, L., M.S. **Twardowski**, and T.J. Cowles. 2000. In situ spectral absorption (ac-9) measurements as an index of photoprotective/photosynthetic carotenoid ratios. *Proceedings from Ocean Optics XV*, October 16-20, Monaco.

Moore, C., M.S. **Twardowski**, and J.R.V. Zaneveld. 2000. The ECO VSF - A multi-angle scattering sensor for determination of the volume scattering function in the backward direction. *Proceedings from Ocean Optics XV*, October 16-20, Monaco.

Twardowski, M.S., E. Boss, J.B. Macdonald, W.S. Pegau, A.H. Barnard, and J.R.V. Zaneveld. 2000. A model for retrieving oceanic particle composition and size distribution from measurements of the backscattering ratio and spectral attenuation. *Proceedings from Ocean Optics XV*, October 16-20, Monaco.

Twardowski, M.S. 2000. Ocean research in the ocean state. *The Rhode Island State Trooper*, 12(1):107-109.

Boss, E., W.S. Pegau, W.D. Gardner, J.R.V. Zaneveld, A.H. Barnard, M.S. **Twardowski**, G.C. Chang, and T.D. Dickey. 2001. Spectral particulate attenuation in the bottom boundary layer of a continental shelf. *J. Geophys. Res.*, 106(C5):9509-9516. [refereed]

Boss, E., M.S. **Twardowski**, and S. Herring. 2001. Shape of the particulate beam attenuation spectrum and its inversion to obtain the shape of the particulate size distribution. *Appl. Opt.*, 40:4885-4893. [refereed]

Dekshenieks, M.M., P.L. Donaghay, J.M. Sullivan, J.E.B. Rines, T.R. Osborn, and M.S. **Twardowski**. 2001. Temporal and spatial occurrence of thin phytoplankton layers in relation to physical processes. *Mar. Ecol. Prog. Ser.*, **223**:61-71. [refereed]

Twardowski, M.S. and A. Barnard. 2001. Observing the ocean: sensing technology and observation platforms. *Maritimes*, 43(4).

Twardowski, M.S., and P.L. Donaghay. 2001. Separating in situ and terrigenous sources of absorption by dissolved material in coastal waters. *J. Geophys. Res.*, 106(C2):2545-2560. [refereed]

Twardowski, M.S., E. Boss, J.B. Macdonald, W.S. Pegau, A.H. Barnard, and J.R.V. Zaneveld. 2001. A model for estimating bulk refractive index from the optical backscattering ratio and the implications for understanding particle composition in Case I and Case II waters. *J. Geophys. Res.*, 106(C7)*:*14,129-14,142. [refereed]

Gould, R., R. Stavn, M. **Twardowski**, and G. Lamella. 2002. Partitioning optical properties into organic and inorganic components from ocean color imagery. *Proceedings from Ocean Optics XVI*, November 18-22, Santa Fe, NM.

Rines, J.E.B., P.L. Donaghay, M. Dekshenieks, J.M. Sullivan, and M.S. **Twardowski**. 2002. Thin layers and camouflage: hidden *Pseudo-nitzschia spp*. (Bacillariophyceae) populations in a fjord in the San Juan Islands, Washington, U.S.A. *Mar. Ecol. Prog. Ser.*, 225:123-137. [refereed]

Sullivan, J.M., M.S. **Twardowski**, P.L. Donaghay, and S. Freeman. 2002. Particulate bulk refractive index distributions in coastal regions as determined from backscattering ratio measurements. *Proceedings from Ocean Optics XVI*, November 18-22, Santa Fe, NM.

Twardowski, M.S., and P.L. Donaghay. 2002. Photobleaching of aquatic dissolved materials: absorption removal, spectral alteration, and their interrelationship. *J. Geophys. Res,* 107(C8). [refereed]

Twardowski, M.S., J.R.V. Zaneveld, and C. Moore. 2002. A novel technique for determining beam attenuation compatible with a small sensor form factor and compact deployment platforms. *Proceedings from Ocean Optics XVI*, November 18-22, Santa Fe, NM.

Zaneveld, J.R.V., M.S**. Twardowski**, K.S. Shifrin, W.S. Pegau, E. Boss, and I. Zolotov. 2002. Inversion of light scattering measurements to obtain biogeochemical parameters. *Proceedings from Ocean Optics XVI*, November 18-22, Santa Fe, NM.

Dekshenieks, M.M., AL Alldredge, A Barnard, E Boss, J Case, TJ Cowles, PL Donaghay, LB Eisner, DJ Gifford, CF Greenlaw, C Herren, DV Holliday, D Johnson, S MacIntyre, D McGehee, TR Osborn, MJ Perry, R Pieper, JEB Rines, DC Smith, JM Sullivan, MK Talbot, MS **Twardowski**, A Weidemann and JR Zaneveld. 2003. Characteristics, Distribution and Persistence of Thin Layers Over a 48 Hour Period. *Mar. Ecol. Prog. Ser.*, 261:1-19. [refereed]

Eisner, L., M.S. **Twardowski**, and T.J. Cowles. 2003. Relationship between phytoplankton pigment composition and in situ spectral absorption measurements in East Sound, Orcas, Island, WA. *Limnol. Oceanogr.,* 48:632-646. [refereed]

Miller, R., M.S. **Twardowski**, C. Moore, and C. Casagrande. 2003. The Dolphin: Technology to Support Remote Sensing Bio-optical Algorithm Development and Applications. *Backscatter* 14(2):8-12. [refereed]

Boss, E., W. S. Pegau, M. Lee, M. S**. Twardowski**, E. Shybanov, G. Korotaev, and F. Baratange. 2004. The particulate backscattering ratio at LEO 15 and its use to study particles composition and distribution. *J. Geophys. Res.*, 109, C01014, doi:10.1029/2002JC001514. [refereed]

Moore, C., J. Da Cuhna, B. Rhoades, M.S. Twardowski, J.R.V. Zaneveld, J. Dombroski. 2004. A new in-situ measurement and analysis system for excitation-emission fluorescence in natural waters. *Proceedings of Ocean Optics XVII*, October 25-29, Freemantle, Australia.

Schofield, O., J. Kohut, J. Kerfoot, L. Creed, C. Mugdal, S. Glenn, M. **Twardowski**, C. Jones, and D. Webb. 2004. Dawn in the age of ocean robots: what can they see? *Proceedings of Ocean Optics XVII*, October 25-29, Freemantle, Australia.

Sullivan, J.M., M.S. **Twardowski**, J.R.V. Zaneveld, C. Moore, B. Rhoades, and R. Miller. 2004. The hyperspectral temperature and salinity dependent absorption coefficients of pure water. *Proceedings of Ocean Optics XVII*, October 25-29, Freemantle, Australia.

Twardowski, M.S., and J.R.V. Zaneveld. 2004. Progress toward a Generalized Optical-Biogeochemical Inversion (GOBI) for natural waters. *Proceedings of Ocean Optics XVII*, October 25-29, Freemantle, Australia.

Twardowski, M.S., E. Boss, J.M. Sullivan, and P.L. Donaghay. 2004. Modeling spectral absorption by chromophoric dissolved organic matter (CDOM**).** *Mar. Chem.,* 89: 69-88, doi:10.1016/j.marchem.2004.02.008. [refereed]

Zaneveld, J.R.V., C. Moore, A.H. Barnard, M.S. **Twardowski**, and G.C. Chang. 2004. Correction and analysis of spectral absorption data taken with the WET Labs AC-S. *Proceedings of Ocean Optics XVII*, October 25-29, Freemantle, Australia.

Sullivan, J.M., M.S. **Twardowski**, Donaghay, P.L., and Freeman, S.A. 2005. Using Scattering Characteristics to Discriminate Particle Types in US Coastal Waters, *Appl. Opt*., 44:1667-1680. [refereed]

Trees, C.C., P.W. Bissett, H,. Dierssen, D.D.R. Kohler, M.A. Moline, J.L. Mueller, R.E. Pieper, M.S. **Twardowski**, and J.R.V. Zaneveld. 2005. Monitoring water transparency and diver visibility in ports and harbors using aircraft hyperspectral remote sensing. *Prodeedings from SPIE Port and Harbor Security Conference*, Vol. 5780, February, Orlando, FL.

Twardowski, M.S., M. Lewis, A. Barnard, J.R.V. Zaneveld. 2005. In-water instrumentation and platforms for ocean color remote sensing applications. *In:* Remote Sensing of Coastal Aquatic Waters, R. Miller and C. Del-Castillo [Eds.], Springer-Kluwer Publishing, pp. 69-100. [refereed]

Twardowski, M.S., J.R.V. Zaneveld, C.M. Moore, J. Mueller, C. Trees, O. Schofield, S. Freeman, T. Helble, and G. Hong. 2005. Diver visibility measured with a compact scattering-attenuation meter (SAM) compatible with AUVs and other small deployment platforms. *Prodeedings from SPIE Port and Harbor Security Conference*, Vol. 5780, February, Orlando, FL.

Zaneveld, J.R.V., M.S. **Twardowski**, M. Lewis, and A. Barnard. 2005. Radiative transfer and remote sensing. *In*: Remote Sensing of Coastal Aquatic Waters, R. Miller and C. Del-Castillo [Eds.], Springer-Kluwer Publishing, pp. 1-20. [refereed]

Aurin, D., H. Dierssen, and M. **Twardowski**. 2006. Absorption, Backscatter and Chlorophyll Algorithms for Ocean Color Remote Sensing in Long Island Sound. *Proceedings of Ocean Optics XVIII*, October 9-13, Montreal, Canada.

Sullivan, J.M., M.S. **Twardowski**, J.R.V. Zaneveld, C. Moore, A. Barnard, P. Donaghay, and B. Rhoades. 2006. The hyperspectral temperature and salinity dependencies of absorption by water and heavy water in the 400-750 nm spectral range. *Appl. Opt.*, 45:5294-5309. [refereed]

Twardowski M., and M. Jonasz. 2006. VSF at the small angles for natural dispersions and power-law slopes (www.tpdsci.com/Tpc/VsfSmlAngNatDspSlp.php). In: *Topics in Particles and Dispersion Science* (www.tpdsci.com). [refereed]

Twardowski M., and M. Jonasz. 2006. Power law in spectral scattering by natural dispersions: Derivation (www.tpdsci.com/Tpc/AtnCfSptPwLwNatDsp.php). In: *Topics in Particles and Dispersion Science* (www.tpdsci.com). [refereed]

Twardowski M., and M. Jonasz. 2006. Power law in spectral scattering by natural dispersions: Finite range of the particle diameter (www.tpdsci.com/Tpc/AtnCfSptPwLwNatDsp.php). In: *Topics in Particles and Dispersion Science* (www.tpdsci.com). [refereed]

Zaneveld, J.R.V, M.S. **Twardowski**, and C. Moore. 2006. Total scattering coefficient meter. *Proceedings of Ocean Optics XVIII*, October 9-13, Montreal, Canada.

Huot, Y., M. Babin, F. Bruyant, C. Grob, M. S. **Twardowski**, and H. Claustre. 2007. Does chlorophyll *a* provide the best index of phytoplankton biomass for primary productivity studies? *Biogeosciences*, 4:853-868, www.biogeosciences.net/4/853/2007 . [refereed]

Huot, Y., A. Morel, M. **Twardowski**, D. Stramski, and R. Reynolds. 2007. Particle optical backscattering along a chlorophyll gradient in the upper layer of the eastern South Pacific. *Biogeosciences*, http://www.biogeosciences-discuss.net/4/4571/2007/bgd-4-4571-2007.pdf [refereed]

Stramski, D., R. Reynolds, M. Babin, H. Claustre, S. Kaczmarek, M. Lewis, R. Rottgers, A. Sciandra, M. Stramska, and M. **Twardowski**. 2007. Relationships POC and optical properties of surface waters in the South Pacific and Atlantic Oceans. *Biogeosciences*, 5, 171-183. [refereed]

Twardowski, M.S., H. Claustre, S.A. Freeman, D. Stramski, and Y. Huot. 2007. Optical backscattering properties of the "clearest" natural waters. *Biogeosciences*, 4, 1041–1058, www.biogeosciences.net/4/1041/2007/. [refereed]

Bell, J., M. **Twardowski**, C. Moore, and A. Barnard. 2008. Comprehensive optical merge processing and acquisition software system (COMPASS) for comprehensive user correction of WET Labs absorption and attenuation data. *Proceedings of Ocean Optics XIX*, October 6-9, Barga, Italy.

Glenn, S., C. Jones, M. **Twardowski**, L. Bowers, J. Kerfoot, J. Kohut, D. Webb, and O. Schofield. 2008. Glider observations of sediment resuspension in a Middle Atlantic Bight fall transition storm. *Limnol. Oceanogr.*, 53(5, part II), 2180-2196.

Moore, C., J. Koegler, W. Strubhar, M. **Twardowski**, A. Barnard, A. Derr, and R. Zaneveld. 2008. The next generation beam attenuation meter (BAM) for autonomous underwater vehicles. *Proceedings of Ocean Optics XIX*, October 6-9, Barga, Italy.

Nencioli, F., G. Chang-Spada, and M. **Twardowski**. 2008. Optical Characterization of an Eddy Induced Diatom Bloom West of the Island of Hawaii. *Proceedings of Ocean Optics XIX*, October 6-9, Barga, Italy.

Sciandre, A., D. Stramski, M. Babin, M. **Twardowski**, and C. Grob. 2008. Diel and spatial variability of particle size distribution in the eastern south Pacific. *Proceedings of Ocean Optics XIX*, October 6-9, Barga, Italy.

Tonizzo, A., J. Zhou, A. Gilerson, T. Iijima, M. **Twardowski**, D. Gray, R. Arnone, B. Gross, F. Moshary, and S. Ahmed .2008. Polarization measurements in coastal waters using hyperspectral multi-angular sensor. *Proceedings of Ocean Optics XIX*, October 6-9, Barga, Italy.

Twardowski, M., S. Freeman, X. Zhang, S. Vagle, and R. Zaneveld. 2008. Resolving surf zone particle dynamics with high sampling rate volume scattering function measurements. *Proceedings of Ocean Optics XIX*, October 6-9, Barga, Italy.

Zhang, X., M. **Twardowski**, C. Hu, and M. Lewis. 2008. Retrieving size and optical properties of individual particle populations from the volume scattering function. *Proceedings of Ocean Optics XIX*, October 6-9, Barga, Italy.

Aurin, D., H.M. Dierssen, M.S. **Twardowski**, and C.S. Roesler. 2009. Optical complexity in Long Island Sound and implications for coastal ocean color remote sensing. *Journal of Geophysical Research*, in press.

Gordon, H.R., M.R. Lewis, S.D. McLean, M.S. **Twardowski**, S.A. Freeman, K.J. Voss, and G.C. Boynton. 2009. Spectra of particulate backscattering in natural waters. *Optics Express*, 17(18), 16192-16208.

Nencioli, F., G. Chang, M. **Twardowski**, and T.D. Dickey. 2009. Optical Characterization of an eddy-induced diatom bloom west of the island of Hawaii. *Biogeosciences*, in press.

Sullivan, J.M., and M.S. **Twardowski**. 2009. Angular shape of the volume scattering function in the backward direction. *Applied Optics*, in press.

Tonizzo, A., J. Zhou, A. Gilerson, M. **Twardowski**, D. Gray, R. Arnone, B. Gross, F. Moshary, and S. Ahmed. 2009. Polarization measurements in coastal waters: hyperspectral and multiangular analysis. *Optics Express*, **17**, 5666-5683.

Voss, K.J., S. McLean, M. Lewis, C. Johnson, S. Flora, M. Feinholz, M. Yarbrough, C. Trees, M. **Twardowski**, and D. Clark. 2009. An example crossover experiment for testing new vicarious calibration techniques for satellite ocean color radiometry. *Journal of Atmospheric and Oceanic Technology*, in press.

Zhang, X., L. Hu, M.S. **Twardowski**, and J.M. Sullivan. 2009. Scattering by solutions of major sea salts. *Optics Express*, in press.

PATENTS

None.

HONORS/AWARDS/PRIZES

Twardowski, M., 2005: *Spinoff* technology selection, NASA Innovative Partnership Program, http://www.sti.nasa.gov/tto/Spinoff2005/PDF/accessible.pdf, p. 62.
Twardowski, M., 2003: Adjunct Professor, University of Rhode Island.
Twardowski, M., 2000: ASEE Visiting Faculty Fellowship, Naval Research Labs.
Twardowski, M., 2000: Early Career Faculty Award, Office of International Research and Development, Oregon State University.
Twardowski, M., 1998: WET Labs Environmental Optics Postdoctoral Fellowship, Oregon State University.